Science of the Total Environment 698 (2020) 134197

Contents lists available at ScienceDirect

Science of the Total Environment

journal homepage: www.elsevier.com/locate/scitotenv

Review

Modeling the degradation and disinfection of water pollutants by photocatalysts and composites: A critical review

Mohamed Ateia [a,*], Mohamed Gar Alalm [b,*], Dion Awfa [c], Matthew S. Johnson [d], Chihiro Yoshimura [c]

[a] Department of Environmental Engineering and Earth Sciences, Clemson University, Clemson, SC 29634, United States
[b] Department of Public Works Engineering, Faculty of Engineering, Mansoura University, Mansoura 35516, Egypt
[c] Department of Civil and Environmental Engineering, School of Environment and Society, Tokyo Institute of Technology, 2-12-1, M1-4, Ookayama, Meguro-ku, Tokyo 152-8552, Japan
[d] Department of Chemistry, University of Copenhagen, Universitetsparken 5, DK-2100 Copenhagen Ø, Denmark

HIGHLIGHTS

- A large set of articles on photocatalytic modeling have been reviewed.
- Current semi-mechanistic models overlook realistic water background components.
- Future models need to be based on experiments under low concentration (ng/L–μg/L).
- New models on compounds other than dyes and *E.coli* need to be developed.

GRAPHICAL ABSTRACT

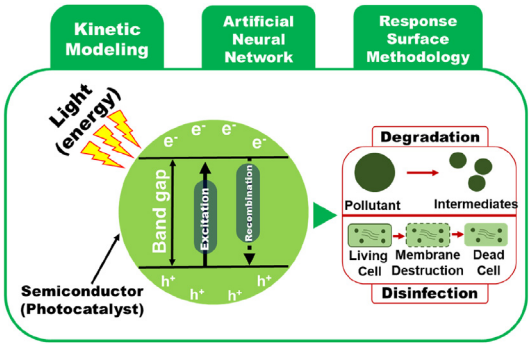

ARTICLE INFO

Article history:
Received 26 April 2019
Received in revised form 20 August 2019
Accepted 29 August 2019
Available online 02 September 2019

Editor: Ching-Hua Huang

Keywords:
Photocatalysis
Kinetic models
Pollutants degradation
Disinfection

ABSTRACT

Recently, a series of new photocatalysts have been developed for to combat diverse bio-recalcitrant contaminants and the inactivation of bacteria. Modeling photocatalytic processes is important to assess these materials, and to understand and optimize their performance. In this study, the recent literature is critically reviewed and analyzed to identify and compare methods of modeling photocatalytic performance. The Langmuir–Hinshelwood model (L-H) has been used in many studies to rationalize the degradation kinetics of single contaminants because it is the simplest model including both the adsorption equilibrium and degradation rates. Other studies report the development of more sophisticated variants of the L-H model that include the rates of catalyst excitation, recombination of electron-hole pairs, production of reactive oxygen species (ROS), and formation of by-products. Modified Chick-Watson (C—W) and Hom models have been used by many researchers to include lag phases of bacteria in the description of disinfection kinetics. Artificial neural networks (ANNs) have been used to analyze the effects of operational conditions on photocatalyst performance. Moreover, response surface methodology (RSM) has been employed for experimental design, and optimization of operational conditions. We have

Abbreviations: AB9, acid blue 9; AC, activated carbon; ANN, Artificial neural networks; AOPs, Advanced oxidation processes; BR46, basic red 46; *C*, Concentration of a contaminant; CAO, Cuckoo optimization algorithm; COD, chemical oxygen demand; DBP, disinfection-by-products; CTA, concentration of TiO_2/AC in water; DB14, Direct blue 14; I_{ave}, the average intensity of incident radiation; *k*, reaction rate coefficient; *K*, equilibrium coefficient; k_{app}, the apparent first-order rate constant.; *L*, the effective path of radiation through the photoreactor; L-H, Langmuir–Hinshelwood; LSSVM, least square support vector machine; MWCNTs, multi-walled carbon nanotubes; NOM, natural organic matter; *R*, the degradation rate; RhB, Rhodamine B; ROS, reactive oxygen species; RSM, response surface methodology; SVM, support vector machine; TOC, total organic carbon; θ_{OH}, the fractional site coverage by hydroxyl radicals; θ_{RhB}, the fractional site coverage by RhB; θ_{TiO2}, the fractional site coverage of TiO_2; ε, the molar absorptivity; μ, specific absorption coefficient of the material.

* Corresponding authors.
E-mail addresses: mohamedateia1@gmail.com (M. Ateia), m_gar_alalm@mans.edu.eg (M.G. Alalm).

https://doi.org/10.1016/j.scitotenv.2019.134197
0048-9697/© 2019 Elsevier B.V. All rights reserved.

Artificial neural network (ANN)
Response surface methodology (RSM)

reviewed and analyzed all available articles that model photocatalytic activity towards water pollution, summarized and put them in context, and recommended future research directions.

© 2019 Elsevier B.V. All rights reserved.

Contents

1. Introduction

Industrial wastewaters contain a variety of toxic and carcinogenic compounds (e.g. pharmaceuticals, pesticides, and surfactants), which pose a threat to the environment if released without treatment; as described in several recent review articles (Félix-Cañedo et al., 2013; Luo et al., 2014; Sousa et al., 2018; Yang et al., 2017). Most of these compounds are persistent and pass through conventional biological treatment systems without significant changes in their chemistry or concentration (Chen et al., 2012). Therefore, advanced water treatment technologies are essential before industrial wastewater containing such compounds can be discharged into the sewer network or water bodies. Advanced oxidation processes (AOPs) are recognized as being effective for the degradation of a variety of bio-recalcitrant compounds including phenols, pesticides, pharmaceuticals, dyes, and petrochemicals (Ambrosio et al., 2017; Awfa et al., 2019; Chen et al., 2017; Faisal et al., 2018; Pal et al., 2018). In AOPs, reactive oxygen species (ROS) oxidize organic molecules and break them down into degradation products. These reactions can be enhanced by light and/or catalysts (Alalm et al., 2015).

Among AOPs, heterogeneous photocatalysts employ solid semiconductor catalysts illuminated at a wavelength of light exceeding the bandgap to degrade organic pollutants. These photocatalysts are able to overcome some of the shortcomings of other AOPs (e.g. sludge formation and the need for pH adjustment) (Koltsakidou et al., 2017). Although TiO_2 and ZnO are the most commonly reported photocatalysts in the literature (Affam and Chaudhuri, 2013), many novel photocatalysts have been developed during the last decade that are able to achieve higher photocatalytic activities than pristine TiO_2 and ZnO, by reducing the band-gap, increasing the active surface area, and enhancing the absorption of visible light (Awfa et al., 2018; Cheng et al., 2015; Koltsakidou et al., 2017; Shimizu et al., 2019). In addition, several studies describe the immobilization of photocatalysts on fixed-media surfaces to improve durability and reduce treatment cost (Alalm et al., 2018; Khavar et al., 2018). However, these physical and chemical modifications alter the material characteristics and activity of the photocatalysts.

Several review articles have discussed the performance, reaction mechanisms, and kinetic modeling of photocatalysts for the degradation of organic contaminants and for photocatalytic disinfection. Due to the significant influence of photocatalysts type, operational conditions, and the nature of contaminants, kinetic models are often used for optimizing the photocatalysis process (Sathishkumar et al., 2013). Blanco-Galvez et al. (2007) reviewed studies on application and reactor designs for solar photocatalytic detoxification and disinfection using TiO_2. Byrne et al. (2011) presented a general overview of solar disinfection (SODIS) and the enhancement modification of SODIS by the addition of TiO_2 (i.e., solar photocatalytic disinfection). Both reviews suggested that solar TiO_2 photocatalysis can be an affordable solution for the removal of organic contaminants, and also microorganism disinfection, in the future. Chong et al., 2010a presented an in-depth review of the application, process parameters, and kinetic modeling of TiO_2 photocatalysis for the removal of organic contaminants and disinfection. In the same year, Dalrymple et al., 2010 reviewed the disinfection mechanisms and the mathematical models (e.g. empirical and mechanistic models) used to fit the photocatalytic disinfection process.

Recently, several innovative approaches for enhancing photocatalytic activity for pollution degradation and disinfection have been affected by modifying the bare photocatalysts creating composite photocatalysts. These modifications affected the photocatalysis mechanism compare with the bare photocatalysts (Awfa et al., 2019; Brame et al., 2015; Chen and Liu, 2016; Dong et al., 2015). Yet, most reviews have focused on the use of simple TiO_2 photocatalysis, and use the simplified Langmuir-Hinshelwood kinetic model (i.e., pseudo-first order) approximation to explain the photocatalytic processes. Moreover, photocatalytic experiments have produced a wide variety of results and it can be extremely challenging to create effective models help optimize photocatalytic activity. Artificial neural networks (ANNs) have been used recently to model photocatalytic efficiency (Jing et al., 2017), followed by the introduction of response surface methodology (RSM) to design experiments and optimize operational conditions (Colombo et al., 2013). Therefore, we believe it is imperative to undertake an insightful study that presents a rigorous review delineating the discrepancies and agreements between the disparate reported models in the literature. To the best of our knowledge, there is currently no review considering the use of kinetic, empirical, and exploratory models for the photocatalytic degradation and disinfection of water for composite materials photocatalysts. Thus, a comprehensive overview of models of photocatalytic remediation of contaminated water would help efforts to optimize and implement photocatalysis. In this paper, we present an

overview of recently developed models of photocatalytic processes for simple and composite photocatalysts. The currently available kinetic models in the literature for photocatalytic oxidation and disinfection are summarized and critically reviewed. Finally, we discuss the use of ANNs and RSM for modeling and optimizing operational parameters.

2. Fundamentals and treatment mechanisms

In heterogeneous photocatalysis, light with an energy that is greater than the band gap (i.e., the energy difference between the valence band and the conduction band in semiconductors), excites the electron from the valence band to the conduction band and creates an electron-hole pair (e^- and h^+) which triggers a series of reactions leading to the photocatalytic degradation of pollutants (Awfa et al., 2018). Electrons and holes on the surface of a semiconductor participate in redox reactions that produce reactive species such as hydroxyl radicals (•OH) and superoxide anion radicals ($\bullet O_2^-$). Hydroxyl radicals and superoxide radicals are very strong ROS that can destroy the bonds of stable and unreactive organic molecules to form organic intermediates, which can be further degraded to CO_2 and H_2O (Matos et al., 2009). The overall process of heterogeneous photocatalysis can be decomposed into five steps (Herrmann, 1999). First, contaminants move from the fluid phase to the interface region of the catalyst by diffusion. Second, contaminants are adsorbed onto the surface of the photocatalysts. Third, a chemical reaction occurs with oxidizing and/or reducing species in the vicinity of the surface. Fourth, by-products desorb. Finally, products are removed from the interface region into the bulk fluid. In addition, due to the production of ROS, photocatalysis is recognized as an effective disinfection process (Lim et al., 2011). The major advantage of using photocatalytic disinfection is the elimination of byproducts (DBPs) that result from using chlorine or other oxidants for water disinfection (Ateia et al., 2019; Chong et al., 2011). In photocatalytic disinfection microorganisms become inactive or dead when ROS attack and break the cell wall and denature proteins finally resulting in a variety of end-products (Farrell et al., 2018; Song et al., 2018). In addition, the physical separation of microorganisms by adsorption was found to play a significant role in disinfection by composite materials (Shimizu et al., 2019). Fig. 1 shows some of the most important mechanisms of the photocatalytic degradation and disinfection of water pollutants.

3. Kinetic models

Models of reaction kinetics can be used to describe the time-dependent relationship between the operating conditions of the system and the degradation rate of organic contaminants and/or the deactivation rate of microorganisms. Previous studies have reported that the photocatalytic degradation/deactivation rate depends on the water chemistry parameters (e.g. pH, water temperature, contaminant concentration, dissolved oxygen, natural organic matter, and inorganic species) and system parameters (e.g. light intensity, light wavelength, catalyst type, and catalyst loading) as reviewed elsewhere (Chong et al., 2010a). Therefore, many researchers attempted to develop models that can describe and evaluate the photocatalytic degradation kinetics. In this section, the kinetic models from the literature are reviewed. Table 1 summarizes the catalysts, target contaminants, model applications and the assumptions behind each model.

3.1. Photocatalytic degradation models

In most photocatalysis studies, the concentration of a single contaminant is monitored at periodic time intervals. The removal of organic contaminants by photocatalysis could be attributed to a mechanism of adsorption onto active sites of the catalyst followed by degradation of a contaminant yielding intermediates and end-products. Accordingly, we introduce the kinetic equations corresponding to this mechanism. The Langmuir–Hinshelwood model (L-H) is a simple kinetic model describing the degradation of a single contaminant by photocatalysis. It includes both adsorption and degradation rates (Alalm et al., 2018), as expressed in Eq. (1).

$$r = -\frac{dC}{dt} = \frac{k_r K_{ad} C}{1 + K_{ad} C} \quad (1)$$

where r is the degradation rate, k_r is the reaction rate constant, C is the initial concentration of the contaminant, and K_{ad} is the adsorption equilibrium constant. It is assumed that the reaction system is in dynamic equilibrium, the reaction is surface mediated, and the competition with intermediate products and reactive species for the occupation of catalyst actives sites is not limiting (Chong et al., 2010b). The r value is dependent on the type and concentration of contaminant, the catalyst material, catalyst loading, and the irradiation flux, through the factors k_r and K_{ad} in Eq. (12). K_{ad} and k_r are dependent on the affinity of the molecule for the surface (Alalm et al., 2015; Koltsakidou et al., 2017). If the removal of the contaminant in the dark for the same catalyst loading is low, removal by adsorption can be neglected. Such cases are often reported for low contaminant concentrations (Herrmann, 1999; Van Doorslaer et al., 2012); the value of K_{ad} is very small, and Eq. (1) can be simplified to Eq. (2), resulting in the pseudo-first-order model:

$$\ln\left(\frac{C_t}{C_o}\right) = k_r K_{ad} t = -k_{app} t \quad (2)$$

where C_0 is the initial concentration of the contaminant, C_t is contaminant concentration at a certain time, k_{app} is the apparent first-

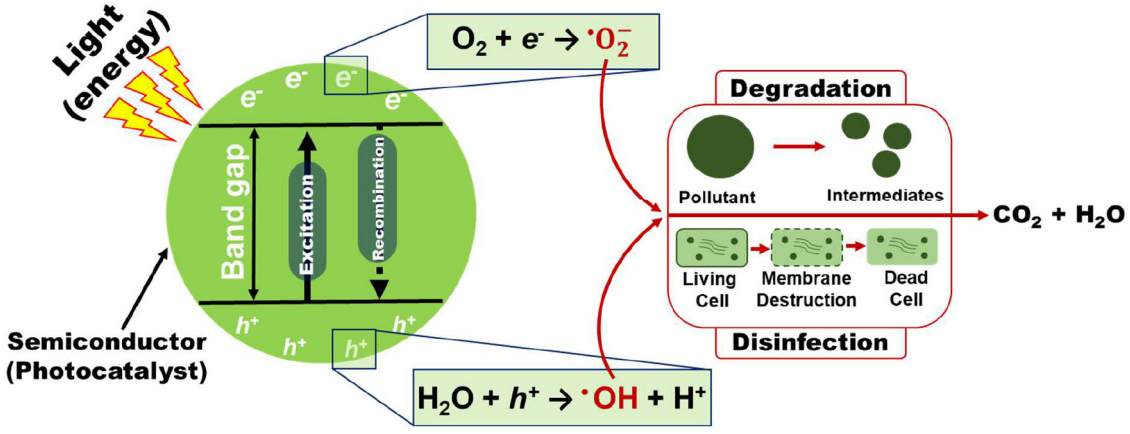

Fig. 1. Key mechanisms in the photocatalytic degradation and disinfection of water pollutants.

Table 1
Overview of photocatalytic degradation kinetics models.

Catalysts	Contaminants	Model applications	Assumptions	R^2	Ref.
Photocatalytic degradation models					
AC-TiO_2	Rhodamine B (RhB - dye)	• Effect of initial concentration of RhB. • Effect of light intensity. • Effect of the ratio of AC to TiO_2.	• Oxidation on the surface of the catalyst. • Radical production (•OH) mainly formed from the adsorbed H_2O molecules. • Faster recombination rate. • •OH concentration is constant at a steady state. • h^+ concentration is constant at a steady state. • Adsorption coefficient for all organic molecules (i.e., parent compound and degradation products) present in the reaction mixture are equal. • Adsorption rate constant is dependent on light intensity. • Does not consider direct oxidation and photolysis reaction. • Photocatalytic reaction experiment was initiated after adsorption-desorption equilibrium was established.	0.95–0.97	(Li et al., 2008)
AC-TiO_2	Rhodamine B (RhB - dye)	• Effect of initial concentration of RhB. • Effect of light intensity. • Effect of the ratio of AC to TiO_2.	• Oxidation on the surface of the catalyst. • Radical production (•OH) mainly formed from the adsorbed H_2O and O_2 molecules. • Faster recombination rate. • •OH concentration is constant at a steady state. • h^+ concentration is constant at a steady state. • Adsorption coefficient for all organic molecules (i.e., parent compound and degradation products) present in the reaction mixture is equal. • Photocatalytic reaction experiment was initiated after adsorption-desorption equilibrium was established. • Does not consider direct oxidation and photolysis reaction.	0.15-15[a]	(Zhang et al., 2011)
ZnO	Acid blue (dye)	• Effect of initial concentration of acid blue. • Effect of light intensity. • Effect of the loading of ZnO.	• Oxidation on the surface of the catalyst. • Radical production (•OH) mainly formed from the adsorbed H_2O. • •OH concentration is constant at a steady state. • h^+ concentration is constant at a steady state. • Fast and slow recombination rate scenarios of h^+-e^-. • Considered degradation products in the reaction. • Photocatalytic reaction experiment was initiated after adsorption-desorption equilibrium was established. • Consider photolysis reaction. • Does not consider direct oxidation.	0.97	(Amani-Ghadim and Dorraji, 2015)
TiO_2	• Furfuryl alcohol • 4-chlorophenol • Diclofenac (pharmaceutical) • 17α-ethynylestradiol (pharmaceutical)	• Inhibitory effect of NOM (e.g. SWNOM) or background constituents (*tert*-butyl alcohol) with different initial concentration.	• Oxidation on the surface of the catalyst and in the bulk solution. • Adsorption rate constant is independent of light intensity. • •OH concentration is constant at a steady state condition. • Does not consider degradation products in the reaction (i.e., first 20 min reaction only). • Photocatalytic reaction experiment was initiated after adsorption-desorption equilibrium was established. • Consider photolysis reaction. • Does not consider direct oxidation. • Consider adsorption competition and inner filter effect.	0.90–0.97	(Brame et al., 2015)
AC-TiO_2	Carbofuran (pesticide)	• Effect of initial concentration of carbofuran.	• Oxidation on the surface of the catalyst. • Radical production (•OH) mainly formed from the adsorbed H_2O and O_2 molecules. • Faster recombination rate. • •OH concentration is constant at a steady state. • h^+ concentration is constant at a steady state. • Adsorption coefficient for all organic molecules (i.e., parent compound and degradation products) present in the reaction mixture is equal. • Photocatalytic reaction experiment was initiated after adsorption-desorption equilibrium was established. • Does not consider direct oxidation and photolysis reaction.	0.93–0.97	(Vishnuganth et al., 2016)
Sm-ZnS	Direct blue 14 (dye)	• Effect of initial concentration of direct blue 14. • Effect of light intensity.	• Empirical kinetic model calculation.	0.9–0.97	(Bakhtkhosh and Mehrizad, 2017)

Table 1 (*continued*)

Catalysts	Contaminants	Model applications	Assumptions	R^2	Ref.
$CNT-ZnSnO_4$	Basic red (dye)	• Effect of the loading of ZnO. • Effect of the loading of pH. • Effect of initial concentration of basic red. • Effect of light intensity.	• Oxidation on the surface of the catalyst. • Radical production (•OH) mainly formed from the adsorbed H_2O. • •OH concentration is constant at a steady state. • h^+ concentration is constant at a steady state. • Considered degradation products in the reaction. • Slow recombination rate scenarios of h^+-e^- due to trapping by water molecules (based on scavenger measurement). • Photocatalytic reaction experiment was initiated after adsorption-desorption equilibrium was established. • Consider direct oxidation and photolysis.	0.99	(Dorraji et al., 2017)
Ag-CNT-ZnS	Rhodamine B (dye)	• Effect of initial concentration of Rhodamine B. • Effect of the loading of Ag-CNT-ZnS.	• Oxidation on the surface of the catalyst. • Radical production (•OH) mainly formed from the adsorbed H_2O. • •OH concentration is constant at a steady state. • h^+ concentration is constant at a steady state. • Considered degradation products in the reaction. • Photocatalytic reaction experiment was initiated after adsorption-desorption equilibrium was established. • Slow recombination rate scenarios of h^+-e^- due to trapping by Ag and CNT.	0.91	(Yazdani and Mehrizad, 2018)
Photocatalytic disinfection models					
$AC-TiO_2$	*E. coli*	• The ratio of TiO_2 to AC • Light intensity • Temperature • pH	• Oxidation on the surface of the catalyst. • Photogenerated oxidants are predominant. Inactivation follows modified Langmuir--Hinshelwood model. • The fractional site coverage by •OH is constant. Adsorption coefficient for all intermediates is equal.	NA	(Youji et al., 2008)
TiO_2, Silica-TiO_2	*E. coli*	• Catalyst concentration The ratio of TiO_2 to silica • The chemical composition of water ($NaCl$, $NaHCO_3$, Na_3PO_4, Humic acid)	• e^- concentration is constant at a steady state. • •OH concentration is constant at a steady state. • h^+ concentration is constant at a steady state. • The bacterial lysis of the inactivated bacteria can generate the same number of organic compounds as the events of reaction. • Rate constants and adsorption constants for all intermediates are equal.	0.99	(Marugán et al., 2008)
H-titanate nanofiber catalyst (mainly TiO_2)	*E. coli*	• Catalyst concentration	• e^- concentration is constant at a steady state. • •OH concentration is constant at a steady state. • h^+ concentration is constant at a steady state. • The bacterial lysis of the inactivated bacteria can generate the same number of organic compounds as the events of reaction. • Rate constants and adsorption constants for all intermediates are equal.	0.97–0.99	(Chong et al., 2011)
TiO_2	*E. coli*	• Catalyst concentration • Initial bacteria concentration • Light intensity	• e^- concentration is constant at a steady state. • •OH concentration is constant at a steady state. • h^+ concentration is constant at a steady state. • The bacterial lysis of the inactivated bacteria can generate the same number of organic compounds as the events of reaction. • Rate constants and adsorption constants for all intermediates are equal.	5.3–7.4[c]	(Marugán et al., 2011)
TiO_2 (continuous reactor)	*E. coli*	• Catalyst concentration • Light intensity (distance from the reactor wall)	• e^- concentration is constant at a steady state. • •OH concentration is constant at a steady state. • h^+ concentration is constant at a steady state. • The bacterial lysis of the inactivated bacteria can generate the same number of organic compounds as the events of reaction. • Rate constants and adsorption constants for all intermediates are equal.	NA	(Marugán et al., 2013)
TiO_2 (& H_2O_2)	*M. aeruginosa*	• Catalyst concentration	• H_2O_2 and *OH under visible light are the major factors contributing to the degradation of cell integrity without any synergistic effect among each other. • Inactivation follows delayed Chick-Watson model and Hom model.	0.90–0.99	(Chang et al., 2018)

order rate constant (min^{-1}), and t is reaction time (min). k_{app} can be used to compare the photodegradation performance of different photocatalysts, discuss the effect of water chemistry, and the influence of operational conditions. For instance, Alalm et al. (2016b) used k_{app} and the L-H model to compare the performance of ZrO_2, WO_3, and their composites including $Ru/WO_3/ZrO_2$ for degradation of the pesticide carbofuran and the antibiotic ampicillin. As shown in Fig. 2, the linear regression slopes between ln (C_0/C) and irradiation time (t) represented the values of k_{app}.

As described in the L-H model, the removal of contaminants by adsorption on photocatalyst particles may be relatively low and can be omitted. When photocatalysts coalesce with supporting materials that have a large specific surface area (e.g. AC, MWCNTs, magnetite, etc.), however, the adsorption can significantly contribute to the removal of contaminants (Ateia et al., 2017a; Ateia et al., 2018; Ateia et al., 2017b; Shimizu et al., 2018). Accordingly, models describing photocatalytic degradation by composites are reviewed separately from other models that describe the degradation by bare photocatalysts.

3.1.1. Degradation models for bare photocatalysts

Due to the non-selective nature of ROS, the photocatalysis should be considered not only in the context of the targeted contaminant, but also taking various inhibition mechanisms in complex water matrices into consideration (Ren et al., 2018). Brame et al. (2015) developed a model to describe the inhibitory effect of background constituents such as natural organic matter (NOM) on the performance of photocatalytic oxidation using bare TiO_2. Their model considers different hindering mechanisms including site blocking due to the adsorption of inhibitors, scavenging of ROS on the catalyst surface and in the solution, and the inner filter effect, which can decrease the efficiency of the photocatalysis. The photodegradation of organic contaminants (e.g. furfuryl alcohol and 4-chlorophenol) without considering the degradation of by-products can be expressed as a second order reaction (Eq. (3)).

$$\frac{dC_A}{dt} = k_A C_{ROS} C_A \tag{3}$$

where C_A is the concentration of the target contaminant, C_{ROS} is the concentration of ROS at steady state, and k_A is the reaction rate constant. A mass-balance approach was taken that includes ROS-mediated degradation in the bulk solution, adsorption on catalyst active sites, and degradation by ROS and/or photo-generated holes. The scavenging of ROS by an inhibitory compound both in the bulk and at the surface was included in the mass balance of ROS. By considering the ROS production rate and the concentration of the inhibitory compound, an overall model for the degradation rate of a target compound (A) was obtained as expressed in Eqs. (4–6).

$$\frac{dC_A}{dt} = \frac{-P_{ROS,0}}{1 + \frac{k_N C_N (F + K_N S)}{k_A C_A (F + K_A S)}} 10^{-\mu l C_N} \tag{4}$$

$$F = \frac{1}{1 + \frac{k_A C_A + k_N C_N}{D\prime}} \tag{5}$$

$$S = \frac{1}{1 + K_A C_A + K_N C_N} \tag{6}$$

where C_A is the concentration of the target compound A, k_A is the reaction rate constant for a specific ROS reacting with A, K_A is the Langmuir adsorption constant for A, C_N is the equilibrium concentration of the inhibition compound N, k_N is the reaction rate constant for a specific ROS reacting with N, K_N is the Langmuir adsorption constant for N, P_{ROS} is the production of ROS, μ is the specific absorption coefficient of the material, l is the optical path length of the incoming light, and D' is the diffusion coefficient normalized per unit diffusion length. For the validation of this model, photocatalytic experiments were conducted using P25 TiO_2, which mainly produces hydroxyl radicals, and amino-functionalized fullerenes attached to a silica gel substrate, which mainly generates superoxide species; for the removal of furfuryl alcohol and 4-chlorophenol (i.e., probe compound) in the presence of NOM and t-BuOH (i.e., inhibitory compound). For all experiments, the model attained a high degree of accuracy in predicting degradation rates in the presence of inhibiting agents.

Amani-Ghadim and Dorraji (2015) developed a pseudo first-order model of the degradation of acid blue 9 (AB9) by ZnO nanoparticles. The degradation rate (r_d) was expressed according to the Eq. (7).

$$r_d = k'[\mathrm{AB9}]_{ads}[\cdot\mathrm{OH}] \tag{7}$$

where $[AB9]_{ads}$ is the dye concentration on the catalysts surface, k' is the reaction rate constant in the equation between •OH radicals and dye, and •OH is the concentration of hydroxyl radicals estimated using the steady-state approximation. The concentration of hydroxyl radicals was estimated by assuming that the hydroxyl radicals are only formed via trapping of positive holes by water molecules. All of the assumptions used in this model are listed in Table 1. Two different recombination rate assumptions were used: a slow regime representing a low concentration of electron-hole pairs and a fast regime for high concentrations of electron-hole pairs. It should be noted that these regime assumptions are thought to occur due to the effect of water molecules on the recombination reaction (i.e., trapping of holes by water molecules could compete with recombination reaction, or not), and also the effects of light intensity and wavelength for the photoexcitation of an electron from the valence band to the conduction band to create an electron-hole pair (e^- and h^+). The models for high and low concentrations of

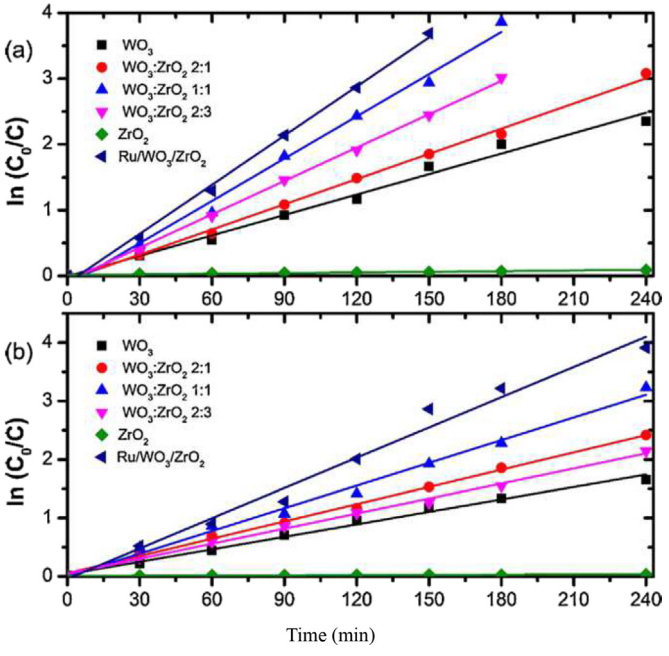

Fig. 2. Typical results of an experiment showing pseudo first order kinetics. Photocatalytic degradation by different catalysts, pH 7, catalyst dosage = 1.0 g/L, carbofuran initial concentration = 20 mg/L, ampicillin initial concentration = 10 mg/L, UV flux = 50 W/m^2, (a) carbofuran, (b) ampicillin (Alalm et al., 2016b).

electron-hole pairs are expressed by Eqs. (8–9) respectively.

$$k_{app,Hhec} = \frac{\beta_{H1} I^{\frac{1}{2}} [ZnO]^{\frac{1}{2}}}{1 + \beta_{H2}[Dye]_0 + \beta_{H3} I^{\frac{1}{2}} [ZnO]^{\frac{1}{2}}} \quad (8)$$

$$k_{app,Lhec} = \frac{\beta_{L1} I^{\frac{1}{2}} [ZnO]^{\frac{1}{2}}}{1 + \beta_{L2}[Dye]_0 + \beta_{L3} I^{\frac{1}{2}} [ZnO]} \quad (9)$$

where β represents factors that depend on the production rate of electron-hole pairs (1), the generation of hydroxyl radicals via trapping of holes by adsorbed water molecules (2), and the reaction rate between hydroxyl radicals and dye molecules and intermediate products (3). The calculated k_{app} values in the 'fast', high electron-pair concentration scenarios showed good agreement with the experimental values ($R^2 = 0.971$). Therefore, the authors concluded that hole trapping by water is not fast enough to inhibit electron-hole recombination in ZnO nanoparticles.

3.1.2. Degradation models for photocatalysts composites

The earliest study was reported by Li et al. (2008) on the development of a kinetic model to describe the removal of rhodamine B (RhB) by a TiO_2/activated carbon (TiO_2/AC) photocatalyst. The model was built using a few key elements; (1) experimental light intensity, (2) the assumption that the adsorption of RhB and its intermediate products are equal, (3) photonic activation step of hole-electron (h^+-e^-), and (4) that the •OH reaction with RhB and intermediates is the rate-limiting step. Accordingly, the degradation rate is represented by Eq. (10).

$$r = k'' \Theta_{OH} \Theta_{RhB} \quad (10)$$

where k'' is the reaction rate coefficient, and Θ_{OH} and Θ_{RhB} are the fractional site coverage by hydroxyl radicals and RhB, respectively. Θ_{OH} and Θ_{RhB} were derived according to the assumption listed in Table 1, and the final model is expressed in Eq. (11).

$$k_r = \frac{k''(K_O k'_4/k_5)(k_1/k_2)^{1/2} I^{1/2}}{1 + (K_O k'_4/k_5)(k_1/k_2)^{1/2} I^{1/2}} \quad (11)$$

where k_1 is reaction rate coefficient representing photoexcitation of TiO_2 to produce electron-hole pairs, k_2 represents electron-hole recombination to produce heat, k_4 describes the reaction between a hole and water, k'_4 is the product of k_4 and the water concentration, k_5 is the reaction between ROS and organic molecules, K_O is the adsorption constant for hydroxyl radicals, and I is the light intensity. The new model fits well with the experimental data and provides insight into the effect of the ratio of TiO_2 to AC on TiO_2/AC photocatalysis.

Based on the work of Li et al. (2008), Zhang et al. (2011) developed a new kinetic model of TiO_2/AC photocatalysis for RhB by considering the adsorption equilibrium constants for intermediates in the expression of degradation rate as depicted in Eq. (12).

$$r = \frac{kK_1 C}{1 + K_1 C + \sum K_i C_i} \quad (12)$$

where K_i is the adsorption equilibrium constant for each intermediate and C_i is the concentration of each intermediate. The final developed model is expressed in Eq. (13).

$$k = \left[\left(\frac{k_4^2}{k'_3} \right)^{\frac{1}{2}} + \left(\frac{k_4^2}{k'_3} \right)^{\frac{1}{2}} \right] k_3^{\frac{1}{2}} \left(1 - \left(1 - \sum \frac{k_{i+1}}{k_{-i}} \right) \theta_{TiO_2} \right) \times \left(\frac{1 - e^{-2.303 L \varepsilon C_{TA} \theta_{TiO_2}}}{L} \right)^{\frac{1}{2}} I_{ave}^{\frac{1}{2}} \quad (13)$$

where k_i is the reverse reaction rate constant for adsorption of each intermediate and catalyst, k_3 is the reaction rate constant in the reaction of irradiated TiO_2 to produce electron-hole pairs, k'_3 is the reaction rate constant in the equation of electron-hole recombination to produce heat, k_4 is the reaction rate constant in the equation between hole and water molecules, θ_{TiO2} is the fractional site coverage of TiO_2, L is the effective path of radiation through the photo-reactor, ε is the molar absorptivity, CTA is the concentration of TiO_2/AC in water, and I_{ave} is the average intensity of incident radiation. This model fitted well with the experimental data and was successfully validated (after the adjustment of some modeling parameters) in another study (TiO_2/AC photocatalysis of methyl orange) (Li et al., 2006). However, it should be noted that any practical application of the system must consider economic constraints in addition to the photodegradation efficiency.

Thus, the most recent study on TiO_2/AC photocatalysis implicitly linked a kinetic model optimizing photodegradation, and electrical energy demand (i.e., economic feasibility) for use on carbofuran (i.e., pesticide) removal (Vishnuganth et al., 2016). The model was developed based on the assumptions of Li et al. (2008) and Zhang et al. (2011). The adsorption coefficients for carbofuran in the reaction mixture were assumed, and the final form of the model is expressed by Eq. (14).

$$r = k_r \frac{k_C C k_0 [\cdot OH]}{(1 + k_C C_0)(1 + k_0 [\cdot OH])} \quad (14)$$

where [•OH] is the concentration of hydroxyl radicals and it is taken to be constant (i.e., Bodenstein steady state assumption). Thus, this model partially resembles the classic L-H model and at low initial carbofuran concentration ($C < 10^{-3}$ M) the equation will follow Eq. (13). The electrical energy determination (E_{EO}) can be calculated using Eq. (15).

$$E_{EO} = \frac{P \times t}{V \times \ln\left(\frac{Ct}{Co}\right)} \quad (15)$$

where P is the rated power of the system, t is the irradiation time, V is the volume of the water in the reactor, and C_o and C_t are the initial and time-dependent concentrations of a pollutant, respectively. This E_{Eo} approach provides the preliminary data for scale-up and also a simple comparison for different photocatalysts (Miklos et al., 2018).

In addition, a number of studies have attempted to enhance the photocatalytic activity of semiconductor materials by incorporating carbon nanotubes (CNT), due to their potentially superior characteristics (e.g. high charge carrier mobility retarding electron-hole recombination, and high specific surface area) (Awfa et al., 2018). However, creating a detailed mechanism for kinetic modeling is still a major challenge. Photocatalytic degradation of contaminants occurs due to the interaction with ROS or via direct oxidation by photogenerated holes (Cavalcante et al., 2016). However, most existing kinetic models seem to have overlooked the latter mechanism. Dorraji et al. (2017) developed a mechanistic model for the degradation of basic red 46 (BR46) by zinc stannate/CNT. Based on experiments carried out by ROS scavengers, it was found that the degradation of BR46 occurred by oxidation by primary photo-generated holes, and oxidation by secondary hydroxyl

radicals. Accordingly, the overall degradation rate was expressed as in Eq. (16).

$$r = \frac{-d[BR46]_t}{dt} = k_{BR46}[h^+][BR46]_{ads} + k_{OH\cdot BR46}[^\circ OH]_{ads}[BR46]_{ads} \quad (16)$$

where k_{BR46} is the rate constant for direct oxidation of BR46 on photo-generated holes, and $k_{OH.BR46}$ is the rate constant for the reaction between hydroxyl radicals and BR46 molecules. The concentrations of hydroxyl radicals and photo-generated holes were calculated using the steady-state approximation. The final model form could be expressed by Eqs. (17–21).

$$r = \frac{\alpha I + \beta I[BR46]_0}{1 + \gamma[BR46]_0}[BR46]_{aq} \quad (17)$$

$$\alpha = \frac{k_{irr}k_{BR46}K_{BR46}}{k\prime_{H_2O}} + \frac{k_{irr}k_{\cdot OH,BR46}K_{BR46}}{k_{inact}} \quad (18)$$

$$\beta = \frac{k_{irr}k_{\cdot OH,BR46}k_{BR46}K^2_{BR46}}{(K_{BR46}+1)k_{inact}k\prime_{H_2O}} + \frac{k_{irr}k_{\cdot OH,Int}k_{BR46}K_{BR46}}{k_{inact}k\prime_{H_2O}} \quad (19)$$

$$\gamma = \frac{k_{\cdot OH,BR46}K_{BR46}}{(K_{BR46}+1)k_{inact}} + \frac{k_{\cdot OH,Int}}{k_{inact}} \quad (20)$$

$$k\prime_{H_2O} = k_{H_2O}[H_2O]_{ads} \quad (21)$$

where $[BR46]_0$ is the initial dye concentration, $[BR46]_{aq}$ is the dye concentration, I is the light intensity, k_{irr} is the reaction rate constant in the equation of catalysts irradiated to produce electron-hole pairs, k_{BR46} is the reaction rate constant in the equation between hole and dye, K_{BR46} is the adsorption rate constant for dye, $k_{\cdot OH,BR46}$ is the reaction rate constant in the equation between •OH radicals and dye, k_{inact} is the reaction rate constant in the equation of •OH radicals changing to OH^- and hole (•OH radicals deactivation), and k_{H2O} in the reaction rate constant in the equation between hole and water molecules. The calculated reaction rates showed good agreement with the experimental rate ($R^2 = 0.99$).

Similarly, Yazdani and Mehrizad (2018) developed a new mechanistic model for Ag-ZnS-CNT photocatalysis for the degradation of rhodamine blue (RhB). In their proposed mechanism (Fig. 3), it was assumed that Ag played a role as a sensitizer by surface plasmon resonance, while MWCNT acted as a sensitizer and also an electron acceptor under visible light irradiation. The electrons from ZnS are photoexcited to the conduction band of ZnS together with electrons from Ag and MWCNT. These electrons react with oxygen to generate superoxide radicals. In the presence of MWCNT, excited electrons move into the graphitic π electron band, inhibiting electron-hole recombination (i.e., decreasing the recombination rate). Moreover, the adsorption affinity and high specific surface area of MWCNTs help to sequester RhB and concentrate it close to photocatalyst active sites. In parallel, holes in the valence band of ZnS contribute to the formation of hydroxyl radicals. Accordingly, the degradation rate is expressed by Eq. (22).

$$R = k_{10}[RhB]_{ads}[\cdot OH] \quad (22)$$

where $[RhB]_{ads}$ is the dye concentration on the catalysts surface, k_{10} is the reaction rate constant in the equation between •OH radicals and dye, and [•OH] is the concentration of hydroxyl radicals estimated using the steady-state approximation. Rates for hole production, the reaction between holes and water to produce hydroxyl radicals, the oxidation of RhB molecules by hydroxyl radicals, and the reaction between intermediates and hydroxyl radicals were included in the model and expressed by Eqs. (23–27).

$$R = \frac{k_1[Ag{-}ZnS{-}MWCNTs]}{k_2[Rh{-}B]_0 + k_3[Ag{-}ZnS{-}MWCNTs] + 1}[Rh{-}B]_{ads} \quad (23)$$

$$k_1 = \frac{k_{10}k_3}{k_{13}} \quad (24)$$

$$k_2 = \frac{k_{10} + k_{11}}{k_{13}} \quad (25)$$

$$k_3 = \frac{k_3k_{12}}{k\prime_8k_{13}} \quad (26)$$

$$k\prime_8 = k_8[H_2O]_{ads} \quad (27)$$

where [Ag-ZnS-MWCNTs] is the catalysts concentration, $[Rh{-}B]_0$ is the initial dye concentration, k_3 is the reaction rate constant for hole production, k_8 is the reaction rate constant in the reaction between hole and water molecules, k_{11} is the reaction rate constant in the reaction between •OH radicals and intermediate, k_{12} is the reaction rate constant in the equation between •OH radicals and electron (•OH radicals deactivation), and k_{13} is the reaction rate constant in the reaction of •OH radicals changing to OH^- and hole (•OH radical deactivation). The model was

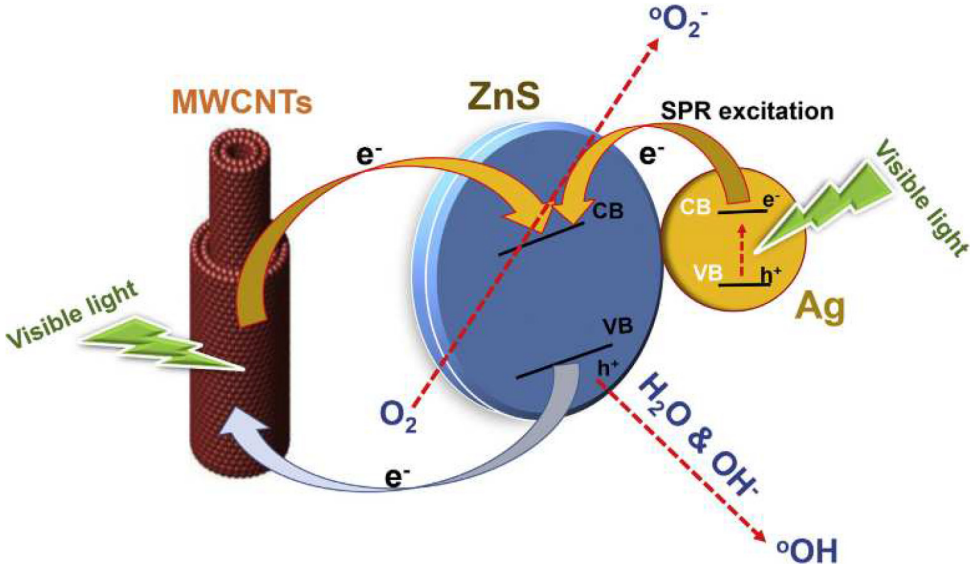

Fig. 3. The proposed photocatalytic mechanism of the Ag-ZnS-MWCNTs under visible light irradiation (Yazdani and Mehrizad, 2018).

then simplified to an L-H form and the comparison between experiment and calculated values of k_{app} showed good agreement ($R^2 = 0.91$).

Several studies have used photocatalytic kinetic modeling for Zn-based photocatalysts. A new, modified k_{app} value (i.e., as a function of pH, catalyst loading, initial contaminant concentration, the mass ratio of ZnS over Sm, and irradiation intensity) has been developed for Sm-doped-ZnS photocatalysis towards the removal of direct blue 14 (DB14) (Bakhtkhosh and Mehrizad, 2017). The modified k_{app} values can be calculated by Eq. (28).

$$k_{app} = k\prime\frac{[ZnS:Sm]_0^a I_0^b}{[DB14]_0^c pH^d} \tag{28}$$

where a, b, c, d, and k' are the exponents of the non-linear equations that can be calculated by regression analysis. The calculated values of k_{app} by this model were notably close to the calculated values from the experimental results and the modified kinetic model revealed that the process was compatible with pseudo-first order kinetics. Further, an empirical relation was used in this study to predict rate constants as a function of water chemistry and operational parameters. However, it should be noted that there is no reason to believe that the models can be extrapolated beyond the range of calibrated values (Dalrymple et al., 2010).

Generally, most studies that report photocatalysis kinetics were performed using synthetic dyes as a proxy for contaminants. However, these tests can mask the partially non-catalytic behavior of the reaction because dye's themselves could be a source of reactivity by electron transfer to the conduction band of the semiconductor (i.e. they act as sensitizers). Best practice is, therefore, to test photocatalysts using different molecules to highlight the photocatalytic activity of the materials (Herrmann, 2010). Currently, available models were developed based on experiments with high initial concentrations of contaminants, in the range of 10^2–10^7 times their typical concentrations in waste streams (Fig. 4). Therefore, more efforts are still needed to develop kinetic models to describe the photocatalytic degradation of pollutants at low concentration levels (i.e. ng/L–μg/L). This will allow elucidating the effect of initial concentration on the model accuracy. It should be noted, however, that the R^2 value indicating goodness of fit is more suitable for linearity testing and is dependent on the number of data points (i.e. the different number of data used in each study can limit the direct comparison among those studies). Another important aspect is that measuring only the disappearance of parent compounds is not recommend because different by-products and intermediates are produced during the photodegradation of organic molecules. Accordingly, the organic concentrations can be expressed collectively using the chemical oxygen demand (COD) or total organic carbon (TOC) to assess the overall degradation (and progress towards mineralization) of pollution; in some cases, the reaction products are more toxic than the original contaminant. A lump-sum L-H model can be used to describe the removal of TOC by a photocatalytic process as expressed by Eq. (29) (Chong et al., 2010b).

$$r_{TOC} = \frac{\beta_1[TOC]}{\beta_2 + \beta_3[TOC]} \tag{29}$$

where β_1, β_2, and β_3 are empirical parameters determined from experimental results.

3.2. Photocatalytic disinfection models

Eq. (30) expresses a general model for the kinetics of photodisinfection. In this model, it is assumed that the photocatalyst concentration is constant during the whole process (Chong et al., 2010b).

$$\frac{dN}{dt} = -k\,m\,N^x\,C^n\,T^{m-1} \tag{30}$$

where N is the number of living bacteria at time t, k is the experimental reaction rate, C is the concentration of photocatalyst, and x, n, and m are

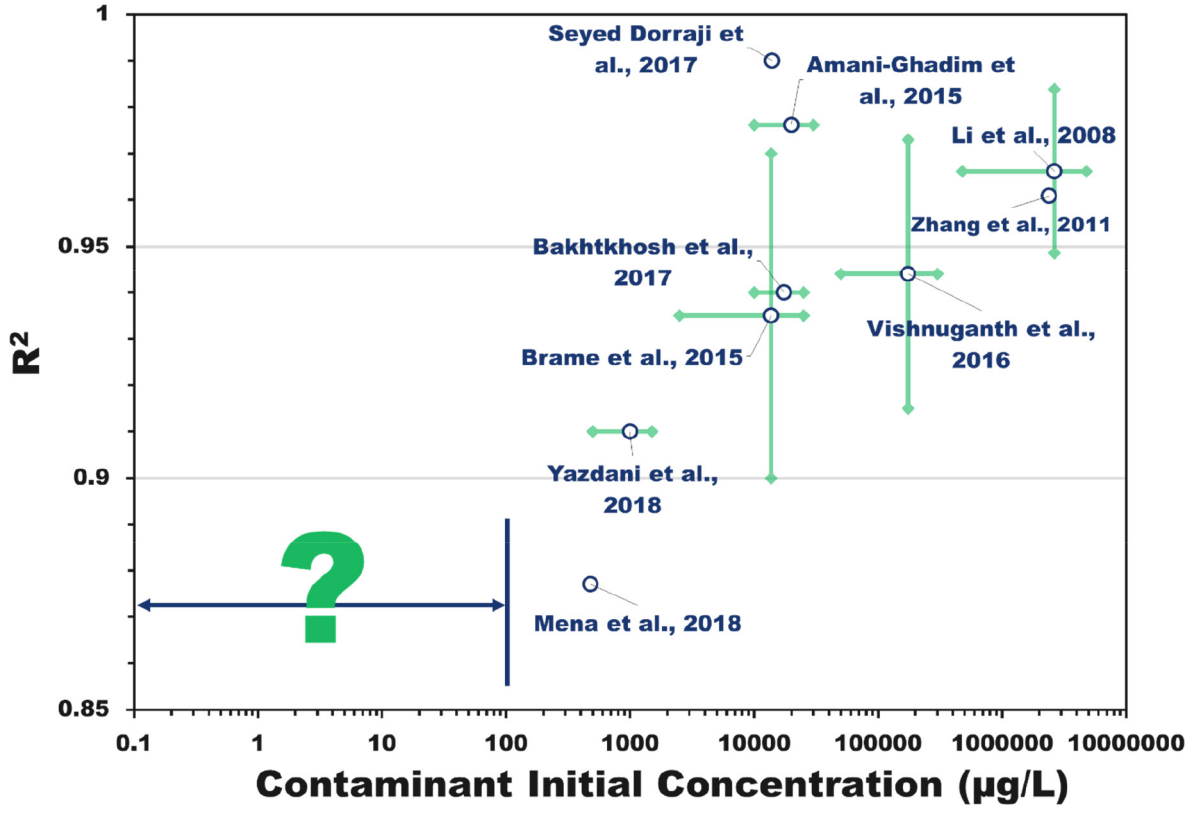

Fig. 4. The relationship between the initial concentration of contaminants and the accuracy of the corresponding developed kinetic degradation models.

the empirical constants of the model. A Chick-Watson (C—W) model (Eq. (31)) has also been used to describe the disinfection rates in photocatalytic processes (Yan et al., 2018).

$$\ln\frac{N}{N_0} = -kt \tag{31}$$

where N_0 is the initial number of living bacteria. The limitation of the classic C—W model is that the disinfection rate is described using a first-order kinetic relationship without considering the catalyst loading.

In addition, the process of removing bacteria by irradiation may exhibit shouldering or tailing if limited inactivation occurs early or late in the process, which is not included in the classic C—W model. To overcome this limitation, Cho et al. (2004) used a delayed C—W model (Eq. (32)), which included a lag phase to describe the possible shoulder in the kinetic relationship, and also considered the concentration of hydroxyl radicals.

$$\ln\frac{N}{N_0} = -k\,(C\,T - C\,T_{lag}) \tag{32}$$

where C is the concentration of hydroxyl radicals, T is the irradiation time, and T_{lag} is the length of the induction or lag phase.

The experimental results showed a lag phase at lower values of C^*T, which supports the use of this model to represent photocatalytic disinfection, however, a fit to the experimental results did not show high correlation, as shown in Fig. 5. To overcome the non-linearity of the disinfection kinetics, Chong et al. (2010b) suggested using the Hom model (Eq. (33)), which predicts the inactivation of bacteria with a non-linear function of catalyst concentration and irradiation time.

$$\log\frac{N}{N_0} = -k'\,C^n\,T^m \tag{33}$$

where k' is the degradation rate, C is the concentration of catalyst, and n and m are empirical parameters that affect the non-linearity of C and T respectively. This model is limited to photocatalytic disinfection because it can only provide two non-linear regions.

Additionally, Li et al. (2008) derived a simple model based on pseudo first order equation (Eq. (34)). In this model, it was assumed that the fractional site coverage by hydroxyl radicals is constant because the dissolved oxygen in the system was not changing.

$$r = k_r \times \frac{k_C C}{1 + k_C C_0} = k_{app} C \tag{34}$$

where k_r is the rate constant, k_C is the adsorption rate constant, C is the bacteria concentration, and C_0 is the initial bacteria concentration.

Marugán et al. (2008) developed a model that takes into consideration shouldering and tailing, and surface inhibition from organic by-products released by the decomposition of bacteria and background organics. A scheme for photocatalytic disinfection was proposed to include the damage of bacteria cells, the inactivation of bacteria, and the production of organic by-products as shown in Eqs. (35–36) (Chong et al., 2011).

$$\frac{dC_{undam}}{dt} = -k\frac{KC_{undam}^n}{1 + KC_{undam}^n + KC_{dam}^n} \tag{35}$$

$$\frac{dC_{dam}}{dt} = k\frac{KC_{undam}^n - KC_{dam}^n}{1 + KC_{undam}^n + KC_{dam}^n} \tag{36}$$

where k is the rate constant, K is the pseudo-adsorption constant, C_{undam} is the undamaged bacteria concentration, C_{dam} is the damaged bacteria concentration, and n is the inhibition coefficient.

We note that this model involves three independent parameters that can be determined by fitting the experimental results. This is the same number of independent parameters as found in empirical models like the Hom model, which is commonly used to fit survival curves including, simultaneously, shoulders and tails. However, in contrast to the limited physical meaning of the parameters appearing in the empirical models, this model gives a substantial meaning to the kinetic (k), interaction (K) and inhibition (n) parameters (Chong et al., 2011). Marugán et al. (2011) developed a rigorous kinetic model including the radiation absorption effects on photocatalytic inactivation of bacteria. To establish different irradiation conditions, a black light blue lamp with a maximum emission at 370–375 nm was used with or without three different neutral polymeric filters. The irradiation intensity was calculated by integration over the wavelength range in which there is an overlap between the photocatalyst absorption and the radiation spectra of the lamp after the attachment of different filters. The model employed a series of processes for the inactivation mechanism including the incremental damages and lysis. The volumetric reaction rates of undamaged and damaged bacteria were expressed by Eqs. (37–38) respectively.

$$R_u = -\alpha_1\left(\frac{K_{ads}C_{cat}}{1 + K_{ads}C_{cat}}\right)\frac{[B_u]^2}{[B_u] + \alpha_4[B_d]} + \alpha_3([B]_0 - [B_u] - [B_d])\left[-1 + \sqrt{1 + \frac{\alpha_2 j}{S_g C_{cat}}}\right] \tag{37}$$

$$R_d = \alpha_1\left(\frac{K_{ads}C_{cat}}{1 + K_{ads}C_{cat}}\right)\frac{[B_u]^2 - \alpha_4[B_d]^2}{[B_u] + \alpha_4[B_d]} + \alpha_3([B]_0 - [B_u] - [B_d])\left[-1 + \sqrt{1 + \frac{\alpha_2 j}{S_g C_{cat}}}\right] \tag{38}$$

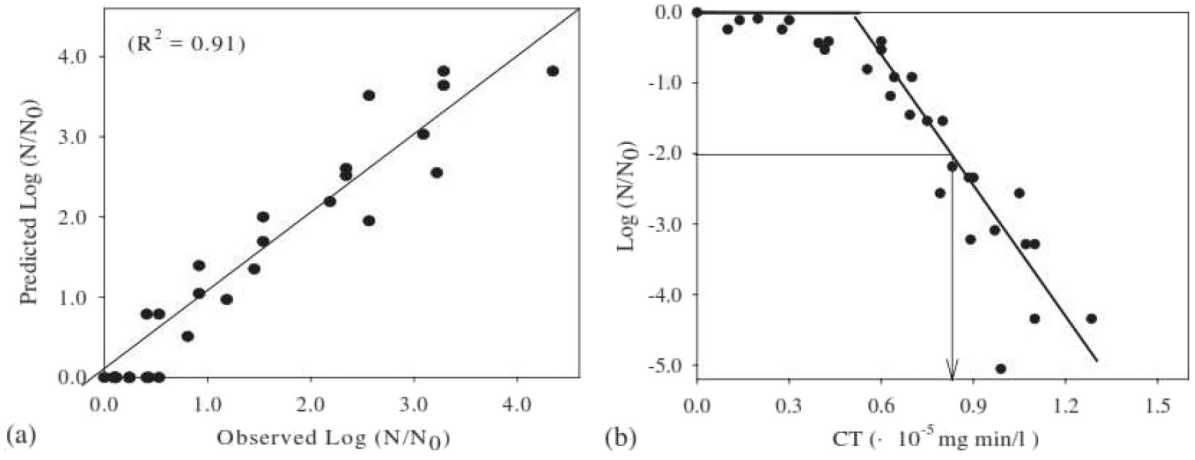

Fig. 5. Delayed Chick-Watson model for inactivation of E.coli, (a) Evaluation of fit; (b) Model prediction (Cho et al., 2004).

where R_u is the reaction rate for undamaged bacteria, R_d is the reaction rate for damaged bacteria, $[B_u]$ is the undamaged bacteria concentration, $[B_d]$ is the damaged bacteria concentration, $[B]_0$ is the initial bacteria concentration, K_{ads} is the equilibrium adsorption constant, C_{cat} is the catalyst concentration, j is the local volumetric rate of photon absorption, S_g is the catalyst specific surface area, and α_1, α_2, α_3, and α_4 are kinetic parameters. The model has been validated by experimental results obtained at different initial bacteria concentrations, catalyst loadings, and irradiation powers. It is suggested that the interaction between microorganisms and catalyst can be considered to be limited, which allowed removing one parameter to simplify the model.

Later, the same group worked to create a new model to simulate photocatalytic disinfection in a bench-scale, annular, continuous flow photo-reactor (Marugán et al., 2013). Mass balance was used to describe the concentration of undamaged and damaged bacteria in the tank. The differential equation describing mass conservation of undamaged and damaged bacteria in the photo-reactor was derived neglecting thermal effects and axial diffusion and assuming azimuthal symmetry, steady state, constant diffusion coefficient, and unidirectional axial flow. The model was then expressed as a function of cylindrical coordinates (Eqs. (39–42)).

$$v_z(r)\frac{\partial[B_u](z,r)}{\partial z} = D\left(\frac{1}{r}\frac{\partial}{\partial r}\left(r\frac{\partial[B_u](z,r)}{\partial r}\right)\right) + R_u(z,r) \tag{39}$$

$$v_z(r)\frac{\partial[B_d](z,r)}{\partial z} = D\left(\frac{1}{r}\frac{\partial}{\partial r}\left(r\frac{\partial[B_d](z,r)}{\partial r}\right)\right) + R_d(z,r) \tag{40}$$

$$v_z(r) = 2\left(1-(r/r_{ext})^2 + \frac{1-\chi^2}{\ln(1/\chi)}\ln(r/r_{ext})\right)/\left(\frac{1-\chi^4}{1-\chi^2} - \frac{1-\chi^2}{\ln(1/\chi)}\right) \tag{41}$$

$$\chi = r_{int}/r_{ext}. \tag{42}$$

where $v_z(r)$ is velocity profiles in the annular space, R_u is the reaction rate for undamaged bacteria, R_d is the reaction rate for damaged bacteria, $[B_u]$ is the undamaged bacteria concentration, $[B_d]$ is the damaged bacteria concentration, z is the axial cylindrical coordinate, r is the radial cylindrical coordinate, r_{int} is the radial cylindrical coordinate relative to the internal wall of the reactor, and r_{ext} is the radial cylindrical coordinate relative to the external wall of the reactor. The validation of the model was carried out graphically by comparing the model prediction curve with the experimental results obtained at different catalyst concentrations (Fig. 6). This model could be used to predict the photocatalytic disinfection performance for similar photo-reactor configurations, taking into consideration the relatively high intrinsic variability of experiments with microorganisms, and that the model parameters were not adjusted.

Chang et al. (2018) developed a sequential reaction model to describe the generation of hydroxyl radicals by H_2O_2 and TiO_2 and quantified their effects on the cell integrity of microcystins and the degradation of microcystins (MCs). First, the delayed Chick-Watson model and the Hom model were employed to simulate the lag behavior of cell damage. Then, kinetic models for describing the concentrations of MCs were developed by integration of a cell rupture kinetic model with an MCs degradation model, assuming that MCs are released into the water immediately after cell rupture, as recommended in previous reports (Huo et al., 2015). In the kinetic models, it was assumed that H_2O_2 and hydroxyl radicals are the main contributors to the rupture of cells under visible light. In addition, the synergistic effect between H_2O_2 and hydroxyl radicals was neglected. Accordingly, the cell rupture kinetics were divided into two parts. A kinetic rate constant was assigned to hydroxyl radicals and another rate constant was assigned to H_2O_2. The refined equations for a dual-oxidant delayed Chick-Watson model and a Hom model are expressed in Eqs. (43–44)

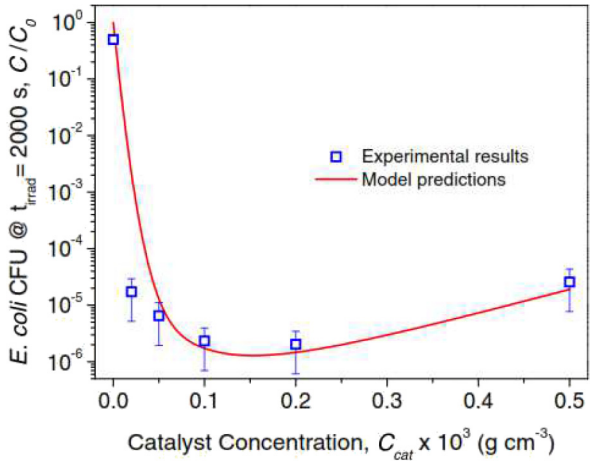

Fig. 6. Comparison between model predictions and interpolated experimental results for the remaining concentration of viable bacteria after 2000 s of irradiation as a function of catalyst concentration (Marugán et al., 2013).

respectively.

$$\ln\frac{N}{N_0} = \begin{cases} 0 \ (t \le t_{lag}) \\ -(k_{C,H_2O_2,cell} + k_{C,\cdot OH,cell}R_{ct})(C_{H_2O_2}t - C_{H_2O_2}t_{lag}) \ (t > t_{lag}) \end{cases} \tag{43}$$

$$\ln\frac{N}{N_0} = \begin{cases} 0 \ (t \le t_{lag}) \\ -(k_{C,H_2O_2,cell} + k_{C,\cdot OH,cell}R_{ct})(C_{H_2O_2}t - C_{H_2O_2}t_{lag}) \ (t > t_{lag}) \end{cases} \tag{44}$$

where t_{lag} is the lag phase time, $k_{C,\ H2O2,\ cell}$ is the second-order rate constant of cell rupture caused by H_2O_2 in a dual-oxidant delayed Chick-Watson model, $k_{C,\ \cdot OH,\ cell}$ is the second-order rate constant of cell rupture caused by •OH in a dual-oxidant delayed Chick-Watson model, $k_{H,\ H2O2,\ cell}$ is the second-order rate constant of cell rupture caused by H_2O_2 in a dual-oxidant Hom model, $k_{H,\ \cdot OH,\ cell}$ is the second-order rate constant of cell rupture caused by •OH in dual-oxidant Hom model, R_{ct} is the radical transformation efficiency, C_{H2O2} is the H_2O_2 concentration, k^* is the first-order decay constant of the disinfectant, and m and n are empirical parameters. Both of the dual-oxidant models were further validated by comparing the predicted values with the values obtained from the experimental work. The validation showed that both models could be used to predict cell rupture of microcystins under different of loadings of H_2O_2 and/photocatalyst (Fawzy et al., 2016).

4. Empirical models

4.1. Artificial neural networks (ANNs)

ANNs are data processing systems that have been developed in analogy to the mechanism of biological nervous systems of the brain (Alalm and Nasr, 2018). They have the ability to discern the relationship between a large number of inputs and their contributions to more than one output. Therefore, ANNs can be very effective in describing and predicting the influence of operating parameters on the degradation efficiency of certain pollutants by photocatalysis. Moreover, the models can be easily constructed using programming software (Fawzy et al., 2016; Nasr et al., 2016). Each ANN consists of a number of neurons grouped in ordered layers. The first layer is the input layer which includes the input (independent) neurons. The final layer is the output layer, which includes one or more dependent variables. In most ANN models of photocatalyst efficiency, the output layer comprises one neuron providing the removal efficiency (Hassani et al., 2018). The layers between the input and output layers are called the hidden layers. The hidden layers provide internal processing in the ANNs to increase their accuracy. In some cases, a single hidden layer is sufficient to obtain the desired

accuracy if the number of neurons is sufficient (Khataee and Kasiri, 2010). Accordingly, the number of neurons in the hidden layer (s) was tested in many models to determine the optimum number, determined using ANN accuracy (Hassani et al., 2018). In a feed-forward ANN, all the neurons of a given layer are directly linked to all the neurons of the next layer. Data processing in ANNs is performed as a weighted summation of the variables obtained from the preceding layer. The weighted summation process is transferred through layers by mathematical equations called activation functions. Khataee and Kasiri (2010) listed many activation functions that can be used in ANNs. However, only three activation functions are widely used in the literature. The first is the hard-limit transfer function which limits the output neuron to the values zero and one (Durán et al., 2007). The second is the linear function, and the third is a sigmoid, which accepts any input value and transforms it into a number between zero and 1 as expressed in Eq. (45).

$$a = \frac{1}{1 + e^n} \tag{45}$$

The quality and reliability of an ANN are strongly dependent on the quality of the experimental data and the structure of the network. The experimental results are used as inputs and in order to validate the outputs, so it is very important to include the most important parameters in the input layer to obtain a reliable network (Radwan et al., 2018). Some recent studies using ANN models to describe photocatalytic processes are summarized in Table 2. It can be seen that ANNs have been applied to experiments using different types of catalysts and a variety of contaminants including phenols, pesticides, and pharmaceuticals. The experimental inputs used in the ANN models varied depending on the nature and purposes of the studies. However, most researchers used at least the irradiation time, catalyst loading, and initial concentration of contaminants as inputs (Dhiman et al., 2017; Ghanbary et al., 2012). Azadi et al. (2018) used the amount of dopant tungsten and the calcination temperature of the catalyst as inputs to incorporate the composition and the preparation method of the catalyst in his model. Jasso-Salcedo et al. (2016) included the wavelength of the irradiating light as an input parameter, to take into account the effect of the type of the light source on the degradation efficiency of bisphenol-A. Other

Table 2
Reviewed ANN models for photocatalytic processes.

Catalyst	Contaminant	Inputs	Outputs	ANN structure	No of epochs	Validation R^2	Ref.
ZnO + H_2O_2 TiO_2 + H_2O_2	Power station effluent	- H_2O_2 concentration - Catalyst loading	- Cyanides degradation constant - Formates degradation constant	Not given	Not given	Not given	(Durán et al., 2007)
TiO_2/montmorillonite	Ciprofloxacin	- Ciprofloxacin concentration - Irradiation time - Catalyst loading - pH - O_3 flow rate	- Ciprofloxacin degradation	5-11-1	21	0.996	(Hassani et al., 2018)
ZnO	AB9	- Catalyst loading - pH - Irradiation time - Irradiation intensity - AB9 concentration	- AB9 degradation	5:9:1	Not given	0.9883	(Amani-Ghadim and Dorraji, 2015)
Polymer capped ZnO	Acridine orange dye	- Acridine orange concentration - Irradiation time - Catalyst loading	- Acridine orange degradation	Not given	Not given	0.9814	(Dhiman et al., 2017)
Ag/ZnO	Bisphenol-A	- Bisphenol-A concentration - pH - Light wavelength	- Bisphenol-A degradation rate	3:8:10:1 3:10:10:1	Not given	0.99922 0.99985	(Jasso-Salcedo et al., 2016)
Tungsten/TiO_2	Landfill leachate	- pH - Irradiation time - Dopant content - Calcination temperature	- COD removal	4:13:1	Not given	0.98	(Azadi et al., 2018)
TiO_2	4-Nitrophenol	- Catalyst loading - Irradiation time - Irradiation intensity - 4-Nitrophenol concentration	- 4-Nitrophenol degradation	4:14:1	4000	0.9925	(Ghanbary et al., 2012)
TiO_2/ZrO_2	Carbamazepine	- Catalyst loading - Irradiation time - pH - Carbamazepine concentration	- Carbamazepine degradation	4:5:1	Not given	0.9975	(Das et al., 2014b)
ZnO/montmorillonite	Disperse red 54	- Catalyst loading - Irradiation time - Disperse red 54 concentration	- Disperse red 54 degradation	3:10:1	Not given	Not given	(Kıranşan et al., 2015)
TiO_2 + Mn^{2+}	Phenol	- Mn^{2+} loading - Irradiation time - pH - Phenol concentration - Applied current	- Phenol degradation	5:12:1	Not given	0.978	(Khataee et al., 2014)
TiO_2	17α-Ethynylestradiol	- Catalyst loading - Irradiation time - 17α-Ethynylestradiol concentration - DOC - Water conductivity	- 17α-Ethynylestradiol degradation	5-13-1	Not given	0.994	(Frontistis et al., 2012)

characteristics such as dissolved organic carbon (DOC) were used as input for the degradation of 17α-ethynylestradiol by TiO_2 (Frontistis et al., 2012). The number of hidden layers was used in most of the reviewed studies, except for the study by Jasso-Salcedo et al. (2016), who used two hidden layers in two models for the degradation of bisphenol-A. In most cases, the number of neurons in the hidden layer is chosen using the minimum value of the mean square error (Das et al., 2014a; Kıranşan et al., 2015). Most of the reported studies used back-propagation to train the ANNs (Khataee et al., 2014). The validation of ANNs for most of the photocatalytic processes of the literature revealed a high correlation between the experimental results and the simulated results as shown in Table 2.

4.2. Response surface methodology (RSM)

A classic method for optimizing operational parameters is to change one parameter while keeping the others constant. This technique consumes time and efforts to search a local area of parameter space (Sahoo and Gupta, 2012). Besides, there is a risk such a search will only locate a local maximum (Giannakis et al., 2017). In contrast, in some cases, RSM can determine optimal operational conditions more quickly by modeling the empirical relationship between the dependent responses, in this context typically removal efficiency, and the independent parameters (input), here the operational conditions (Alalm et al., 2016a; Ateia et al., 2016; Khodadoost et al., 2017; Ng et al., 2016). RSM models comprise a variety of mathematical and statistical equations that can link the operational parameters and optimize the design of experiments (Karimifard and Moghaddam, 2018; Mirzaei et al., 2018). RSM is an advanced technique for fitting mathematical models to the obtained experimental results. These mathematical models may include linear, quadratic, or polynomial equations, etc. (Karimifard and Moghaddam, 2018; Pirsaheb et al., 2018; Rakhshaee and Darvazeh, 2017). An experimental design strategy is used to obtain an appropriate set of data that can be effectively used in an RSM. The most prevalent designs are full factorial, central composite, Box-Behnken, Doehlert, and Taguchi orthogonal array (Khatri et al., 2016). In full factorial design, a set of two or three levels of variables is considered at low, medium, and high values. The main limitation of full factorial design is the production of a large number of combinations which can make the experimental work infeasible logistically. The central composite design comprises three types of data namely center, axial, and cube. The method requires fewer lab experiments so may be able to overcome the interaction problems that occur in full factorial design (Karimifard and Moghaddam, 2018). In Box-Behnken design, the number of points is reduced by replacing some of the extreme values for operational conditions (corner points) with average values. In contrast to the others, Box-Behnken prefers second order polynomials; one limitation is that this design is not preferred for data sets that require the consideration of wide ranges of inputs. The Doehlert design uses a variable space with circular coordinates for two parameters, spherical for three parameters, and hyper-spherical for more than three parameters. It is more appropriate for simulating second-order relations because it is more uniform and the data sets can be easily upgraded by adding a few experimental results, even in the case of an unequal number of points in different levels (Bezerra et al., 2008). In Taguchi orthogonal array design, the number of required experiments is pre-determined to minimally cover the considered parameters to reduce the number of experimental runs (Chong et al., 2010a). Among twelve reviewed papers (Table 3), the central composite design was used in nine, Box-Behnken in two, and Taguchi orthogonal array in nine. Full factorial and Doehlert were not used in any of these papers, possibly because of the large number of experiments required for RSM models. In the majority of the reviewed studies, three inputs were employed in the experimental design. The initial contaminant concentration, the pH of the solution, and the catalyst loading were the most prevalent parameters (Abdullah et al., 2012; Soleymani et al., 2015). Other researchers included the amount of other chemical reagents such as H_2O_2 (Pirsaheb et al., 2018; Secula et al., 2008). In some studies, the aeration rate of the solution was also employed as an input parameter (Ng et al., 2016). Perhaps surprisingly the light intensity was only considered as an input parameter in one of the reviewed studies (Liu and Chiou, 2005). We note that light sources provide constant irradiation in most photocatalytic studies, although the light intensity is not standardized between studies. In addition, most of the researchers employed constant irradiation time to simplify their models and reduce the number of required samples. However, Chong et al. (2010b) considered the irradiation time in addition to contaminant concentration and catalyst loading, in modeling Congo red removal by Taguchi orthogonal array design. The numbers of experiments ranged between 9 and 30, and the mode value was 20 experiments, which was used in four of the reviewed studies. In all studies, RSM showed a high correlation as R^2 ranged between 0.93 and 0.99, which suggests the suitability of RSM for modeling photocatalytic degradation processes.

5. Exploratory models

There are some other models that have been used in the literature with a lesser extent such as exploratory models. In these models, the analysis includes multiple hypotheses about the studied system by widening the assumptions of the models (Agusdinata and Dittmar, 2007). Support vector machine (SVM) is one of the exploratory intelligent techniques that have been used to describe and optimize the photocatalytic degradation. For instance, Mahmoodi et al. (2019) used SVM supported with least square (LSSVM) method and Cuckoo Optimization Algorithm (COA) to describe and optimize the photocatalytic degradation of Reactive Red 198 using a nano-composite of activated carbon and metal-organic framework. The model showed moderate agreement between experimental and predicted results ($R^2 = 0.948$), which suggests the need for future investigations of this method to obtain a better description of photocatalytic processes.

6. Conclusions and recommendations

We have reviewed and analyzed a large set of articles that model the activity of simple and composite photocatalysts towards water pollution. The models are useful for describing the performance of the photocatalysts and allow comparison between different catalysts and operational conditions. Theoretical kinetic models were effectively used to describe the degradation efficiency of pollutants or microorganisms and relate the suggested degradation mechanism with the experimental results. However, involving the operating parameters leads to complexity and hence several assumptions are required to overcome the complex equations. On the other hand, empirical models offer simple equations to describe the influence of operating parameters on degradation efficiency, but it requires long sets of experimental results. Moreover, they are always limited to the studied ranges of inputs. The L-H model is simple and very effective for the description of degradation kinetics. However, many researchers developed more advanced models in order to include additional reactions in the photocatalytic mechanism. Photocatalytic disinfection has been widely simulated in the literature using C—W and Hom models, which can be developed to include the lag phases of bacteria. In addition, some researchers developed even more detailed kinetic models to include the effects of operational conditions and reaction intermediates. ANNs showed high accuracy in the simulation of the influence of operational parameters on the photocatalytic degradation efficiency. The composition of ANNs in recent studies have been reviewed and discussed. It can be also concluded that RSM is effective for modeling, designing, and optimizing photocatalytic experiments. The central composite design was the most prevalent experimental design strategy that had been used to develop an effective RSM model with a minimum number of experiments.

Table 3
Reviewed RSM models for photocatalytic processes.

Catalyst	Contaminant	Inputs	Outputs	Method	No of points	R^2	Reference
ZnO@g-C_3N_4	Sulfamethoxazole	- pH - Catalyst loading - Air flow rate	- Sulfamethoxazole degradation	CCD	20	0.9896	(Mirzaei et al., 2018)
Nano carbon dots	Phenol	- Irradiation time - Catalyst loading - H_2O_2 amount	- Phenol degradation	CCD	18	0.96–0.98	(Pirsaheb et al., 2018)
$Bi_4Ti_3O_{12}$	Tetracycline	- Temperature - pH - Irradiation time	- Tetracycline degradation	BBD	14	0.9929	(Khodadoost et al., 2017)
ZnO	Palm oil mill effluent	- Initial COD - O_2 flow rate - Catalyst loading	- COD removal	CCD	24	0.93	(Ng et al., 2016)
Fe_3O_4 zeolite 13×	Biebrich Scarlet	- Biebrich Scarlet concentration - pH - Catalyst loading	- Biebrich Scarlet degradation	CCD	20	0.9804	(Khatri et al., 2016)
TiO_2	Direct red 16	- pH - Catalyst loading - Direct red 16 concentration	- Direct red 16 degradation	CCD	20	Not given	(Soleymani et al., 2015)
$BiVO_4$	Methylene Blue	- pH - Catalyst loading - Methylene Blue concentration	- Methylene Blue degradation	CCD	17	0.9845	(Abdullah et al., 2012)
Ag-TiO_2	Methylene Blue	- pH - Catalyst loading - Methylene blue concentration	- COD removal - Color removal	BBD	15	0.9999–0.9994	(Sahoo and Gupta, 2012)
H-titanate nanofibe	Congo red	- Catalyst loading - Irradiation time - Congo red concentration - Aeration rate	- Congo red degradation	TOAD	9	0.9994	(Chong et al., 2010b)
TiO_2	Chloramphenicol	- pH - Catalyst loading - Chloramphenicol concentration	- Chloramphenicol degradation	CCD	20	0.9519	(Zhang et al., 2010)
TiO_2-Fe^{3+}–H_2O_2	Dyestuff effluent	- TiO_2 loading - Fe^{3+} loading - H_2O_2 loading	- Decolorization rate	CCD	16	Not given	(Secula et al., 2008)
TiO_2	Red 239	- Light intensity - Stirring speed - Red 239 concentration - Catalyst loading	- Decolorization rate	CCD	30	0.9841	(Liu and Chiou, 2005)

BBD: Box-Behnken design; CCD: Central composite design; TOAD: Taguchi orthogonal array design.

The published studies in the literature show strong progress in the water treatment by photocatalytic systems over the past decade, as demonstrated by their ability to disinfect and purify water under increasingly demanding conditions, along with a deeper theoretical understanding of the mechanism of reactivity. However, contradictory descriptions and models of photocatalytic activity limit further progress. Optimization, especially for real world devices, depends on effective parameterization. In order to achieve that goal, we recommend further studies focused on the following directions:

- In most photocatalytic degradation kinetic models, researchers only considered the effect of initial contaminant concentrations, light intensities, catalyst concentration, pH, and temperature in ultrapure water solutions to develop mechanistic models. However, many of them are in fact semi-mechanistic models that do not include other factors which could reasonably impact the photocatalytic activity and mechanism, such as 1) the intrinsic characteristics of photocatalysts, 2) the effect of background water chemistry (e.g. DO, quality and quantity of contaminants, NOM, and inorganic species), and 3) the effect of system parameter (e.g. the effect of different wavelength). Research is needed to understand the fundamental mechanisms (e.g. radical sources that participated in the reaction and varying environmental conditions) of photocatalytic degradation and photocatalytic disinfection to provide basic information for guiding photocatalytic kinetic modeling and providing a more reliable kinetic model.
- The majority of current studies have used synthetic dyes as the target contaminant. However, this should be avoided because these dyes can themselves act as a source of photocatalytic activity. Moreover, most investigations have used a high concentration of contaminants (mg/L scale) which may skew the results. Determination of the performance of kinetic models under low concentration (ng L^{-1} or μg/L) is a high priority.
- In the photocatalytic disinfection kinetic model, researchers put focus on *E.coli* as a targeted contaminant. Development of photocatalytic disinfection kinetic model for other types of bacteria and viruses with extensive fundamental mechanism can be helpful for future studies of photocatalytic disinfection kinetic modeling.

Declaration of Competing Interest

No conflict of interest exists.

Acknowledgments

Dion Awfa is grateful for a scholarship from Indonesia Endowment Fund for Education (LPDP). This work was supported by JSPS KAKENHI (Grant Number 18H01566) and LPDP. The authors would like to thank Mr. Yuta Shimizu, Tokyo Institute of Technology for the help with the data collection.

References

Abdullah, A.H., Moey, H.J.M., Yusof, N.A., 2012. Response surface methodology analysis of the photocatalytic removal of methylene blue using bismuth vanadate prepared via polyol route. J. Environ. Sci. 24 (9), 1694–1701.

Affam, A.C., Chaudhuri, M., 2013. Degradation of pesticides chlorpyrifos, cypermethrin and chlorothalonil in aqueous solution by TiO2 photocatalysis. J. Environ. Manag. 130, 160–165.

Agusdinata, D.B., Dittmar, L., 2007. System-of-Systems Perspective and Exploratory Modeling to Support the Design of Adaptive Policy for Reducing Carbon Emission. IEEE, pp. 1–8.

Alalm, M.G., Nasr, M., 2018. Artificial intelligence, regression model, and cost estimation for removal of chlorothalonil pesticide by activated carbon prepared from casuarina charcoal. Sustainable Environment Research 28 (3), 101–110.

Alalm, M.G., Tawfik, A., Ookawara, S., 2015. Comparison of solar TiO2 photocatalysis and solar photo-Fenton for treatment of pesticides industry wastewater: operational conditions, kinetics, and costs. Journal of Water Process Engineering 8, 55–63.

Alalm, M.G., Nasr, M., Ookawara, S., 2016a. Assessment of a novel spiral hydraulic flocculation/sedimentation system by CFD simulation, fuzzy inference system, and response surface methodology. Sep. Purif. Technol. 169, 137–150.

Alalm, M.G., Ookawara, S., Fukushi, D., Sato, A., Tawfik, A., 2016b. Improved WO3 photocatalytic efficiency using ZrO2 and Ru for the degradation of carbofuran and ampicillin. J. Hazard. Mater. 302, 225–231.

Alalm, M.G., Samy, M., Ookawara, S., Ohno, T., 2018. Immobilization of S-TiO2 on reusable aluminum plates by polysiloxane for photocatalytic degradation of 2, 4-dichlorophenol in water. Journal of water process engineering 26, 329–335.

Amani-Ghadim, A., Dorraji, M.S., 2015. Modeling of photocatalyatic process on synthesized ZnO nanoparticles: kinetic model development and artificial neural networks. Appl. Catal. B Environ. 163, 539–546.

Ambrosio, E., Lucca, D.L., Garcia, M.H., de Souza, M.T., Freitas, T.K.d.S., de Souza, R.P., Visentainer, J.V., Garcia, J.C., 2017. Optimization of photocatalytic degradation of biodiesel using TiO2/H2O2 by experimental design. Sci. Total Environ. (58), 1, 1–9.

Ateia, M., Nasr, M., Ikeda, A., Okada, H., Fujii, M., Natsuike, M., Yoshimura, C., 2016. Nonlinear relationship of near-bed velocity and growth of riverbed periphyton. Water 8 (10), 461.

Ateia, M., Apul, O.G., Shimizu, Y., Muflihah, A., Yoshimura, C., Karanfil, T., 2017a. Elucidating adsorptive fractions of natural organic matter on carbon nanotubes. Environmental Science & Technology 51 (12), 7101–7110.

Ateia, M., Koch, C.B., Jelavić, S., Hirt, A.M., Quinson, J., Yoshimura, C., Johnson, M.S., 2017b. Green and facile approach for enhancing the inherent magnetic properties of carbon nanotubes for water treatment application. PLoS One 7, 1–21.

Ateia, M., Ceccato, M., Budi, A., Ataman, E., Yoshimura, C., Johnson, M.S., 2018. Ozone-assisted regeneration of magnetic carbon nanotubes for removing organic water pollutants. Chem. Eng. J. 335, 384–391.

Ateia, M., Erdem, C.U., Ersan, M.S., Ceccato, M., Karanfil, T., 2019. Selective removal of bromide and iodide from natural waters using a novel AgCl-SPAC composite at environmentally relevant conditions. Water Res. 156, 168–178.

Awfa, D., Ateia, M., Fujii, M., Johnson, M.S., Yoshimura, C., 2018. Photodegradation of pharmaceuticals and personal care products in water treatment using carbonaceous-TiO2 composites: a critical review of recent literature. Water Res. 142, 26–45.

Awfa, D., Ateia, M., Fujii, M., Yoshimura, C., 2019. Novel magnetic carbon nanotube-TiO2 composites for solar light photocatalytic degradation of pharmaceuticals in the presence of natural organic matter. Journal of Water Process Engineering 31, 100836.

Azadi, S., Karimi-Jashni, A., Javadpour, S., 2018. Modeling and optimization of photocatalytic treatment of landfill leachate using tungsten-doped TiO2 nano-photocatalysts: application of artificial neural network and genetic algorithm. Process Saf. Environ. Prot. 117, 267–277.

Bakhtkhosh, P., Mehrizad, A., 2017. Sonochemical synthesis of Sm-doped ZnS nanoparticles for photocatalytic degradation of Direct Blue 14: experimental design by response surface methodology and development of a kinetics model. J. Mol. Liq. 240, 65–73.

Bezerra, M.A., Santelli, R.E., Oliveira, E.P., Villar, L.S., Escaleira, L.A., 2008. Response surface methodology (RSM) as a tool for optimization in analytical chemistry. Talanta 76 (5), 965–977.

Blanco-Galvez, J., Fernández-Ibáñez, P., Malato-Rodríguez, S., 2007. Solar photocatalytic detoxification and disinfection of water: recent overview. Journal of solar energy engineering 129 (1), 4–15.

Brame, J., Long, M., Li, Q., Alvarez, P., 2015. Inhibitory effect of natural organic matter or other background constituents on photocatalytic advanced oxidation processes: mechanistic model development and validation. Water Res. 84, 362–371.

Byrne, J.A., Fernandez-Ibanez, P.A., Dunlop, P.S., Alrousan, D., Hamilton, J.W., 2011. Photocatalytic enhancement for solar disinfection of water: a review. International Journal of Photoenergy 2011.

Cavalcante, R.P., Dantas, R.F., Bayarri, B., González, O., Giménez, J., Esplugas, S., Junior, A.M., 2016. Photocatalytic mechanism of metoprolol oxidation by photocatalysts TiO2 and TiO2 doped with 5% B: primary active species and intermediates. Appl. Catal. B Environ. 194, 111–122.

Chang, C.-W., Huo, X., Lin, T.-F., 2018. Exposure of Microcystis aeruginosa to hydrogen peroxide and titanium dioxide under visible light conditions: modeling the impact of hydrogen peroxide and hydroxyl radical on cell rupture and microcystin degradation. Water Res. 141, 217–226.

Chen, S., Yan, R., Zhang, X., Hu, K., Li, Z., Humayun, M., Qu, Y., Jing, L., 2017. Photogenerated electron modulation to dominantly induce efficient 2, 4-dichlorophenol degradation on BiOBr nanoplates with different phosphate modification. Appl. Catal. B Environ. 209, 320–328.

Chen, Y., Liu, K., 2016. Preparation and characterization of nitrogen-doped TiO2/diatomite integrated photocatalytic pellet for the adsorption-degradation of tetracycline hydrochloride using visible light. Chem. Eng. J. 302, 682–696.

Chen, Z., Ngo, H.H., Guo, W., 2012. A critical review on sustainability assessment of recycled water schemes. Sci. Total Environ. 426, 13–31.

Cheng, X., Wang, P., Liu, H., 2015. Visible-light-driven photoelectrocatalytic degradation of diclofenac by N, S–TiO2/TiO2 NTs photoelectrode: performance and mechanism study. Journal of environmental chemical engineering 3 (3), 1713–1719.

Cho, M., Chung, H., Choi, W., Yoon, J., 2004. Linear correlation between inactivation of E. coli and OH radical concentration in TiO2 photocatalytic disinfection. Water Res. 38 (4), 1069–1077.

Chong, M.N., Jin, B., Chow, C.W., Saint, C., 2010a. Recent developments in photocatalytic water treatment technology: a review. Water Res. 44 (10), 2997–3027.

Chong, M.N., Zhu, H., Jin, B., 2010b. Response surface optimization of photocatalytic process for degradation of Congo Red using H-titanate nanofiber catalyst. Chem. Eng. J. 156 (2), 278–285.

Chong, M.N., Jin, B., Saint, C.P., 2011. Using H-titanate nanofiber catalysts for water disinfection: understanding and modelling of the inactivation kinetics and mechanisms. Chem. Eng. Sci. 66 (24), 6525–6535.

Colombo, R., Ferreira, T.C., Alves, S.A., Carneiro, R.L., Lanza, M.R., 2013. Application of the response surface and desirability design to the lambda-cyhalothrin degradation using photo-Fenton reaction. J. Environ. Manag. 118, 32–39.

Dalrymple, O.K., Stefanakos, E., Trotz, M.A., Goswami, D.Y., 2010. A review of the mechanisms and modeling of photocatalytic disinfection. Appl. Catal. B Environ. 98 (1–2), 27–38.

Das, L., Maity, U., Basu, J.K., 2014a. The photocatalytic degradation of carbamazepine and prediction by artificial neural networks. Process Saf. Environ. Prot. 92 (6), 888–895.

Das, R., Hamid, S.B.A., Ali, M.E., Ismail, A.F., Annuar, M., Ramakrishna, S., 2014b. Multifunctional carbon nanotubes in water treatment: the present, past and future. Desalination 354, 160–179.

Dhiman, N., Singh, A., Verma, N.K., Ajaria, N., Patnaik, S., 2017. Statistical optimization and artificial neural network modeling for acridine orange dye degradation using in-situ synthesized polymer capped ZnO nanoparticles. J. Colloid Interface Sci. 493, 295–306.

Dong, H., Zeng, G., Tang, L., Fan, C., Zhang, C., He, X., He, Y., 2015. An overview on limitations of TiO2-based particles for photocatalytic degradation of organic pollutants and the corresponding countermeasures. Water Res. 79, 128–146.

Dorraji, M.S., Amani-Ghadim, A., Rasoulifard, M., Taherkhani, S., Daneshvar, H., 2017. The role of carbon nanotube in zinc stannate photocatalytic performance improvement: experimental and kinetic evidences. Appl. Catal. B Environ. 205, 559–568.

Durán, A., Monteagudo, J., San Martín, I., García-Peña, F., Coca, P., 2007. Photocatalytic degradation of pollutants from Elcogas IGCC power station effluents. J. Hazard. Mater. 144 (1–2), 132–139.

Faisal, M., Harraz, F.A., Ismail, A.A., El-Toni, A.M., Al-Sayari, S., Al-Hajry, A., Al-Assiri, M., 2018. Polythiophene/mesoporous SrTiO3 nanocomposites with enhanced photocatalytic activity under visible light. Sep. Purif. Technol. 190, 33–44.

Farrell, C., Hassard, F., Jefferson, B., Leziart, T., Nocker, A., Jarvis, P., 2018. Turbidity composition and the relationship with microbial attachment and UV inactivation efficacy. Sci. Total Environ. 624, 638–647.

Fawzy, M., Nasr, M., Abdel-Gaber, A., Fadly, S., 2016. Biosorption of Cr (VI) from aqueous solution using agricultural wastes, with artificial intelligence approach. Sep. Sci. Technol. 51 (3), 416–426.

Félix-Cañedo, T.E., Durán-Álvarez, J.C., Jiménez-Cisneros, B., 2013. The occurrence and distribution of a group of organic micropollutants in Mexico City's water sources. Sci. Total Environ. 454, 109–118.

Frontistis, Z., Daskalaki, V.M., Hapeshi, E., Drosou, C., Fatta-Kassinos, D., Xekoukoulotakis, N.P., Mantzavinos, D., 2012. Photocatalytic (UV-A/TiO2) degradation of 17α-ethynylestradiol in environmental matrices: experimental studies and artificial neural network modeling. J. Photochem. Photobiol. A Chem. 240, 33–41.

Ghanbary, F., Modirshahla, N., Khosravi, M., Behnajady, M.A., 2012. Synthesis of TiO2 nanoparticles in different thermal conditions and modeling its photocatalytic activity with artificial neural network. J. Environ. Sci. 24 (4), 750–756.

Giannakis, S., Jovic, M., Gasilova, N., Gelabert, M.P., Schindelholz, S., Furbringer, J.-M., Girault, H., Pulgarin, C., 2017. Iohexol degradation in wastewater and urine by UV-based Advanced Oxidation Processes (AOPs): process modeling and by-products identification. J. Environ. Manag. 195, 174–185.

Hassani, A., Khataee, A., Fathinia, M., Karaca, S., 2018. Photocatalytic ozonation of ciprofloxacin from aqueous solution using TiO2/MMT nanocomposite: nonlinear modeling and optimization of the process via artificial neural network integrated genetic algorithm. Process Saf. Environ. Prot. 116, 365–376.

Herrmann, J.-M., 1999. Heterogeneous photocatalysis: fundamentals and applications to the removal of various types of aqueous pollutants. Catal. Today 53 (1), 115–129.

Herrmann, J.-M., 2010. Photocatalysis fundamentals revisited to avoid several misconceptions. Appl. Catal. B Environ. 99 (3–4), 461–468.

Huo, X., Chang, D.-W., Tseng, J.-H., Burch, M.D., Lin, T.-F., 2015. Exposure of microcystis aeruginosa to hydrogen peroxide under light: kinetic modeling of cell rupture and simultaneous microcystin degradation. Environmental science & technology 49 (9), 5502–5510.

Jasso-Salcedo, A.B., Meimaroglou, D., Hoppe, S., Pla, F., Escobar-Barrios, V.A., 2016. Surface modification and immobilization in poly (acrylic acid) of Ag/ZnO for photocatalytic degradation of endocrine-disrupting compounds. J. Appl. Polym. Sci. 133 (25).

Jing, L., Chen, B., Wen, D., Zheng, J., Zhang, B., 2017. Pilot-scale treatment of atrazine production wastewater by UV/O3/ultrasound: factor effects and system optimization. J. Environ. Manag. 203, 182–190.

Karimifard, S., Moghaddam, M.R.A., 2018. Application of response surface methodology in physicochemical removal of dyes from wastewater: a critical review. Sci. Total Environ. 640, 772–797.

Khataee, A., Kasiri, M., 2010. Artificial neural networks modeling of contaminated water treatment processes by homogeneous and heterogeneous nanocatalysis. J. Mol. Catal. A Chem. 331 (1–2), 86–100.
Khataee, A., Fathinia, M., Zarei, M., Izadkhah, B., Joo, S., 2014. Modeling and optimization of photocatalytic/photoassisted-electro-Fenton like degradation of phenol using a neural network coupled with genetic algorithm. J. Ind. Eng. Chem. 20 (4), 1852–1860.
Khatri, K., Klein, J.A., White, M.R., Grant, O.C., Leymarie, N., Woods, R.J., Hartshorn, K.L., Zaia, J., 2016. Integrated omics and computational glycobiology reveal structural basis for influenza A virus glycan microheterogeneity and host interactions. Mol. Cell. Proteomics 15, 1895–1912.
Khavar, A.H.C., Moussavi, G., Mahjoub, A.R., Satari, M., Abdolmaleki, P., 2018. Synthesis and visible-light photocatalytic activity of In, S-TiO2@ rGO nanocomposite for degradation and detoxification of pesticide atrazine in water. Chem. Eng. J. 345, 300–311.
Khodadoost, S., Hadi, A., Karimi-Sabet, J., Mehdipourghazi, M., Golzary, A., 2017. Optimization of hydrothermal synthesis of bismuth titanate nanoparticles and application for photocatalytic degradation of tetracycline. Journal of Environmental Chemical Engineering 5 (6), 5369–5380.
Kıranşan, M., Khataee, A., Karaca, S., Sheydaei, M., 2015. Artificial neural network modeling of photocatalytic removal of a disperse dye using synthesized of ZnO nanoparticles on montmorillonite. Spectrochim. Acta A Mol. Biomol. Spectrosc. 140, 465–473.
Koltsakidou, A., Antonopoulou, M., Evgenidou, E., Konstantinou, I., Giannakas, A., Papadaki, M., Bikiaris, D., Lambropoulou, D., 2017. Photocatalytical removal of fluorouracil using TiO2-P25 and N/S doped TiO2 catalysts: a kinetic and mechanistic study. Sci. Total Environ. 578, 257–267.
Li, Y., Li, X., Li, J., Yin, J., 2006. Photocatalytic degradation of methyl orange by TiO2-coated activated carbon and kinetic study. Water Res. 40 (6), 1119–1126.
Li, Y., Sun, S., Ma, M., Ouyang, Y., Yan, W., 2008. Kinetic study and model of the photocatalytic degradation of rhodamine B (RhB) by a TiO2-coated activated carbon catalyst: effects of initial RhB content, light intensity and TiO2 content in the catalyst. Chem. Eng. J. 142 (2), 147–155.
Lim, T.-T., Yap, P.-S., Srinivasan, M., Fane, A.G., 2011. TiO2/AC composites for synergistic adsorption-photocatalysis processes: present challenges and further developments for water treatment and reclamation. Crit. Rev. Environ. Sci. Technol. 41 (13), 1173–1230.
Liu, H.-L., Chiou, Y.-R., 2005. Optimal decolorization efficiency of Reactive Red 239 by UV/TiO2 photocatalytic process coupled with response surface methodology. Chem. Eng. J. 112 (1–3), 173–179.
Luo, Y., Guo, W., Ngo, H.H., Nghiem, L.D., Hai, F.I., Zhang, J., Liang, S., Wang, X.C., 2014. A review on the occurrence of micropollutants in the aquatic environment and their fate and removal during wastewater treatment. Sci. Total Environ. 473, 619–641.
Mahmoodi, N.M., Abdi, J., Taghizadeh, M., Taghizadeh, A., Hayati, B., Shekarchi, A.A., Vossoughi, M., 2019. Activated carbon/metal-organic framework nanocomposite: preparation and photocatalytic dye degradation mathematical modeling from wastewater by least squares support vector machine. J. Environ. Manag. 233, 660–672.
Marugán, J., van Grieken, R., Sordo, C., Cruz, C., 2008. Kinetics of the photocatalytic disinfection of Escherichia coli suspensions. Appl. Catal. B Environ. 82 (1–2), 27–36.
Marugán, J., Van Grieken, R., Pablos, C., Satuf, M.L., Cassano, A.E., Alfano, O.M., 2011. Rigorous kinetic modelling with explicit radiation absorption effects of the photocatalytic inactivation of bacteria in water using suspended titanium dioxide. Appl. Catal. B Environ. 102 (3–4), 404–416.
Marugán, J., Van Grieken, R., Pablos, C., Satuf, M.L., Cassano, A.E., Alfano, O.M., 2013. Modeling of a bench-scale photocatalytic reactor for water disinfection from laboratory-scale kinetic data. Chem. Eng. J. 224, 39–45.
Matos, J., Garcia, A., Cordero, T., Chovelon, J.-M., Ferronato, C., 2009. Eco-friendly TiO 2–AC photocatalyst for the selective photooxidation of 4-chlorophenol. Catal. Lett. 130 (3–4), 568–574.
Miklos, D.B., Remy, C., Jekel, M., Linden, K.G., Drewes, J.E., Hübner, U., 2018. Evaluation of advanced oxidation processes for water and wastewater treatment–a critical review. Water Res. 139, 118–131.
Mirzaei, A., Yerushalmi, L., Chen, Z., Haghighat, F., 2018. Photocatalytic degradation of sulfamethoxazole by hierarchical magnetic ZnO@ g-C3N4: RSM optimization, kinetic study, reaction pathway and toxicity evaluation. J. Hazard. Mater. 359, 516–526.
Nasr, M., Ateia, M., Hassan, K., 2016. Artificial intelligence for greywater treatment using electrocoagulation process. Sep. Sci. Technol. 51 (1), 96–105.
Ng, K.H., Cheng, Y.W., Khan, M.R., Cheng, C.K., 2016. Optimization of photocatalytic degradation of palm oil mill effluent in UV/ZnO system based on response surface methodology. J. Environ. Manag. 184, 487–493.
Pal, D., Lavania, R., Srivastava, P., Singh, P., Srivastava, K., Madhav, S., Mishra, P., 2018. Photo-catalytic degradation of methyl tertiary butyl ether from wastewater using CuO/CeO2 composite nanofiber catalyst. Journal of Environmental Chemical Engineering 6 (2), 2577–2587.
Pirsaheb, M., Moradi, S., Shahlaei, M., Farhadian, N., 2018. Application of carbon dots as efficient catalyst for the green oxidation of phenol: kinetic study of the degradation and optimization using response surface methodology. J. Hazard. Mater. 353, 444–453.
Radwan, M., Gar Alalm, M., Eletriby, H., 2018. Optimization and modeling of electro-Fenton process for treatment of phenolic wastewater using nickel and sacrificial stainless steel anodes. Journal of water process engineering 22 (1), 155–162.
Rakhshaee, R., Darvazeh, J., 2017. Comparing performance of three forms of hematite in fixed bed reactor for a photocatalytic decolorization: experimental design, model fitting and optimization of conditions. Process Saf. Environ. Prot. 107, 122–137.
Ren, M., Drosos, M., Frimmel, F.H., 2018. Inhibitory effect of NOM in photocatalysis process: explanation and resolution. Chem. Eng. J. 334, 968–975.
Sahoo, C., Gupta, A., 2012. Optimization of photocatalytic degradation of methyl blue using silver ion doped titanium dioxide by combination of experimental design and response surface approach. J. Hazard. Mater. 215, 302–310.
Sathishkumar, P., Mangalaraja, R.V., Anandan, S., Ashokkumar, M., 2013. Photocatalytic degradation of ternary dye mixture in aqueous environment using gold nanoparticles loaded amino and mercapto functionalized TiMCM-41 nanocatalysts in the presence of visible light. Sep. Purif. Technol. 102, 67–74.
Secula, M., Suditu, G., Poulios, I., Cojocaru, C., Cretescu, I., 2008. Response surface optimization of the photocatalytic decolorization of a simulated dyestuff effluent. Chem. Eng. J. 141 (1–3), 18–26.
Shimizu, Y., Ateia, M., Yoshimura, C., 2018. Natural organic matter undergoes different molecular sieving by adsorption on activated carbon and carbon nanotubes. Chemosphere 203, 345–352.
Shimizu, Y., Ateia, M., Wang, M., Awfa, D. and Yoshimura, C. (2019) Disinfection mechanism of E. coli by CNT-TiO2 composites: photocatalytic inactivation vs. physical separation. Chemosphere.
Soleymani, A.R., Saien, J., Chin, S., Le, H.A., Park, E., Jurng, J., 2015. Modeling and optimization of a sono-assisted photocatalytic water treatment process via central composite design methodology. Process Saf. Environ. Prot. 94, 307–314.
Song, K., Taghipour, F., Mohseni, M., 2018. Microorganisms inactivation by continuous and pulsed irradiation of ultraviolet light-emitting diodes (UV-LEDs). Chem. Eng. J. 343, 362–370.
Sousa, J.C., Ribeiro, A.R., Barbosa, M.O., Pereira, M.F.R., Silva, A.M., 2018. A review on environmental monitoring of water organic pollutants identified by EU guidelines. J. Hazard. Mater. 344, 146–162.
Van Doorslaer, X., Heynderickx, P.M., Demeestere, K., Debevere, K., Van Langenhove, H., Dewulf, J., 2012. TiO2 mediated heterogeneous photocatalytic degradation of moxifloxacin: operational variables and scavenger study. Appl. Catal. B Environ. 111, 150–156.
Vishnuganth, M., Remya, N., Kumar, M., Selvaraju, N., 2016. Photocatalytic degradation of carbofuran by TiO2-coated activated carbon: model for kinetic, electrical energy per order and economic analysis. J. Environ. Manag. 181, 201–207.
Yan, Y., Zhou, X., Lan, J., Li, Z., Zheng, T., Cao, W., Zhu, N., Liu, W., 2018. Efficient photocatalytic disinfection of Escherichia coli by N-doped TiO2 coated on coal fly ash cenospheres. J. Photochem. Photobiol. A Chem. 367, 355–364.
Yang, Y., Ok, Y.S., Kim, K.-H., Kwon, E.E., Tsang, Y.F., 2017. Occurrences and removal of pharmaceuticals and personal care products (PPCPs) in drinking water and water/sewage treatment plants: a review. Sci. Total Environ. 596, 303–320.
Yazdani, E.B., Mehrizad, A., 2018. Sonochemical preparation and photocatalytic application of Ag-ZnS-MWCNTs composite for the degradation of Rhodamine B under visible light: experimental design and kinetics modeling. J. Mol. Liq. 255, 102–112.
Youji, L., Mingyuan, M., Xiaohu, W., Xiaohua, W., 2008. Inactivated properties of activated carbon-supported TiO2 nanoparticles for bacteria and kinetic study. J. Environ. Sci. 20 (12), 1527–1533.
Zhang, J., Fu, D., Xu, Y., Liu, C., 2010. Optimization of parameters on photocatalytic degradation of chloramphenicol using TiO2 as photocatalyist by response surface methodology. J. Environ. Sci. 22 (8), 1281–1289.
Zhang, W., Li, Y., Wang, C., Wang, P., 2011. Kinetics of heterogeneous photocatalytic degradation of rhodamine B by TiO2-coated activated carbon: roles of TiO2 content and light intensity. Desalination 266 (1–3), 40–45.